Cement and Concrete Research 102 (2017) 68–89

Contents lists available at ScienceDirect

Cement and Concrete Research

journal homepage: www.elsevier.com/locate/cemconres

cemff: A force field database for cementitious materials including validations, applications and opportunities

Ratan K. Mishra[a,*], Aslam Kunhi Mohamed[b], David Geissbühler[b], Hegoi Manzano[c], Tariq Jamil[d], Rouzbeh Shahsavari[e,*], Andrey G. Kalinichev[f,k], Sandra Galmarini[g], Lei Tao[e], Hendrik Heinz[d], Roland Pellenq[h], Adri C.T. van Duin[i], Stephen C. Parker[j], Robert J. Flatt[a], Paul Bowen[b,*]

[a] Department of Civil, Environmental and Geomatic Engineering, ETH Zurich, CH-8093 Zürich, Switzerland
[b] Powder Technology Laboratory (LTP), EPFL Lausanne, CH-1015 Lausanne, Switzerland
[c] Condensed Matter Physics Department, University of the Basque Country, UPV/EHU, 48080 Bilbao, Spain
[d] Department of Chemical and Biological Engineering, University of Colorado Boulder, Boulder, CO 80303-0596, USA
[e] Department of Civil and Environmental Engineering, Rice University, Houston, TX 77005, USA
[f] Laboratoire SUBATECH (UMR-6457), Institut Mines-Télécom Atlantique, F-44307 Nantes, France
[g] Building Science and Technology, Eidgenössische Materialprüfungs- und Forschungsanstalt (EMPA), CH-8600 Dübendorf, Switzerland
[h] Department of Civil and Environmental Engineering, Massachusetts Institute of Technology, 77 Massachusetts Av., Cambridge, 02139, MA, USA
[i] Department of Mechanical and Nuclear Engineering, The Pennsylvania State University, University Park, PA 16802, USA
[j] Department of Chemistry, University of Bath, Claverton Down, Bath BA2 7AY, United Kingdom
[k] International Laboratory for Supercomputer Atomistic Modelling and Multi-Scale Analysis, National Research University Higher School of Economics, Moscow, Russia

ARTICLE INFO

Keywords:
Cement force field database (***cemff***)
Force field (FF)
Parameterizations
Molecular simulation
Nanoscale mechanisms

ABSTRACT

This paper reviews atomistic force field parameterizations for molecular simulations of cementitious minerals, such as tricalcium silicate (C_3S), portlandite (CH), tobermorites (model C-S-H). Computational techniques applied to these materials include classical molecular simulations, density functional theory and energy minimization. Such simulations hold promise to capture the nanoscale mechanisms operating in cementitious materials and guide in performance optimization. Many force fields have been developed, such as Born–Mayer–Huggins, InterfaceFF (IFF), ClayFF, CSH-FF, CementFF, GULP, ReaxFF, and UFF. The benefits and limitations of these approaches are discussed and a database is introduced, accessible via a web-link (http://cemff.epfl.ch). The database provides information on the different force fields, energy expressions, and model validations using systematic comparisons of computed data with benchmarks from experiment and from ab-initio calculations. The ***cemff*** database aims at helping researchers to evaluate and choose suitable potentials for specific systems. New force fields can be added to the database.

1. Introduction

Cement is one of the most important materials in the construction industry and it has been used for concrete production for over 2000 years. Concrete is the largest material by volume used by mankind. Its use is expected to double in the next 30 years. Therefore, the advancement in the understanding of new concrete formulations is still a very active research area and a substantial amount of research has been focused on the development of high performance sustainable materials towards the emission reduction of greenhouse gases from the cement industry.

Currently cement production contributes about 6–8% of yearly man-made global CO_2 emissions [1,2]. In the production of cement about 60% of the CO_2 emissions comes from the decomposition of limestone ($CaCO_3$) which is almost 80% of the raw material for cement manufacture. Reduction of this, "*chemical*" CO_2 means using less calcium oxide in the cement. This can be achieved by using new alternative materials (calcined clays, limestone, waste products such as fly ash, slag and silica fume) [3–5]. However, such additions change the chemistry and reactivity, and may have consequences on the mechanical properties as well as durability of cement and concrete structures [6–8]. A key factor will be to guarantee the new material reactivity and durability as concrete structures are expected to last for decades. This can only come from a profound scientific understanding of the cementitious materials and their behavior, starting from the atomistic level and then going from the microscale to the macroscale by

* Corresponding authors.
E-mail addresses: rkmishra@ethz.ch (R.K. Mishra), Rouzbeh@rice.edu (R. Shahsavari), paul.bowen@epfl.ch (P. Bowen).

http://dx.doi.org/10.1016/j.cemconres.2017.09.003
Received 20 April 2017; Received in revised form 16 August 2017; Accepted 8 September 2017
Available online 06 October 2017
0008-8846/

integrating the information gained from atomistic simulations.

1.1. Why atomistic scale simulations are interesting?

There are many aspects of cement and concrete behavior that would benefit from a better understanding at the atomistic level [3],

i) Dissolution of the anhydrous clinker and growth of the solid hydrous cement phases [9–16]
ii) Interaction of chemical additives with anhydrous and hydrous cement phases [17–20]
iii) Influence of replacing clinker with locally available materials (clays, waste materials and recycled materials) which influences the chemistry, hydration dynamics, effect on microstructure development [4–7,21]
iv) Degradation mechanisms in cement and concrete (corrosion of steel re-inforcements, freeze thaw and sulfate attack) [22–24]
v) Mechanism of waste/cement interactions (storage of radioactive and non-radioactive waste) [25–28]
vi) Understanding the dependence of mechanical and fracture characteristics due to anisotropy, hardness, dislocation dynamics, porosity and impurities, etc. [29–35]

All of these phenomena deal with chemistry at interfaces at the nanoscale level – the mechanisms behind the above mentioned points are poorly understood even if some knowledge of the microscopic level chemistry is well documented. To be able to predict properties at early ages, durability and degradation phenomena, we need a concerted bottom up approach, with effort at both the atomistic scale to give accurate inputs into microstructural models [36–38] which will then feed mesoscale continuum models [19,39] that are already well developed. With this better understanding of atomistic scale mechanisms, experimental work at the larger concrete testing scale will be better directed and more efficient, eliminating much of the “test and try” methodology. This will allow precise understanding and thus help to achieve a satisfactory reduction in carbon footprint associated with cementitious systems.

1.2. State of the art

The use of atomistic modeling has made great progress over recent years in many different fields, for example, chemical reactivity, crystal growth, ion speciation, inorganic-organic interfaces, molecular recognition, self-assembly, mechanical and thermal properties [40–47]. This progress has made it possible to start simulating different phases related to hydrated cement, namely portlandite [44–46,48] and tobermorite as a calcium silicate hydrate (C-S-H) model, anhydrous as well as hydrous cementitious phase interfaces [40,43,49–55] and interfacial chemical reactions [40,45,56–58].

There has however been some discussion as to the accuracy and comparability of these atomistic simulations both between each other and when confronted with experiment [59,60]. Part of this is perhaps, for the atomistic simulation results at least, due to a lack of a simple way to compare results when looking at different systems using different empirical potentials (Born–Mayer–Huggins (BMH) [54], ClayFF [44], CSH-FF [43], CementFF [46], GULP [61], INTERFACE [51], ReaxFF [62], and UFF [63]). These empirical potentials with accurate parameterizations are the heart of atomistic force field models, and need to be able to give a correct representation of chemical bonding via covalent and ionic interactions [47,64,65].

1.3. Difficult to compare which potential is the best for which situation

One approach to eliminate these shortcomings would be to create a database of force fields used for atomistic simulations with cementitious systems which allows their comparison. Such a database together with a training set or a set of benchmarks (either experimental or from ab-initio simulations) with which the strengths and limitations of the different force fields could be estimated, would help to give a more coherent approach. This would aid tremendously in comparing and evaluating the accuracy and compatibility of the approaches. Such a database would eliminate the re-investigation and validations of force fields already tested and allow a quicker and better choice for future work. The development of such a database and illustration of its use for a series of benchmarks is the subject of this paper. A generalized approach to parameterizing the atomistic models without proper validations can fail to achieve the targeted accuracy and reliability. General purpose force fields like UFF and DREIDING have not been validated to reproduce the physical and chemical properties of specific compounds, and therefore have limited application in cementitious systems [66,67].

1.4. Brief overview of ***cemff*** database

We first give a brief description of the different empirical force fields that have been used for the comparison of the benchmarks before describing the organization of the database. Then the results for the benchmarks chosen using each of the force fields, e.g. properties such as crystal structure, elastic, interfacial and thermal properties, for 3 solids of great importance in cementitious systems namely: tobermorite (model C-S-H, C: CaO, S: SiO_2, and H: H_2O), portlandite (CH) and tricalcium silicate (C_3S) are compared. Finally examples of where the selected force fields are best suited are illustrated highlighting how the database can help researchers to choose the best path towards answering an atomistic scale problem by simulation techniques in cementitious systems.

2. Force field database

The ***cemff*** (http://cemff.epfl.ch) database provides an online library of user-contributed force fields, calculation input files and benchmarking data, aimed at quick comparison of how different force fields perform in a given situation (Fig. 1). The library takes the form of a web-application with a simple and intuitive user interface allowing consultation and editing of the different items stored in the database. Currently there is no specialized force field database available for cement minerals, which is the motivation behind the development of ***cemff***. Presently OpenKIM [68] and NIST [69] repositories provides force field parameters for elements, alloys, mixtures and semiconductor compounds. But cement minerals are very complex minerals which requires a specific set of force field parameters to validate each mineral. ***cemff*** can collect all types of force field models created for cement minerals by researchers around the world and provide the benefits and limitations of each atomistic force field model.

On a technical level, the web-application is based on a custom python back-end, built around the Flask framework [70], querying an SQL database whose items are exposed as python objects to the back-end via the SQLAlchemy library [71]. The user interface is minimalistic by design and decorated by the industry-standard Bootstrap CSS code. Description text fields allow formatted structured input using the Markdown syntax [72] (list, links, emphasis) together with a MathJax [73] parser for easy input of complex mathematical expressions via the LaTeX syntax. The SQL database has several tables, such as ‘Forcefields’, ‘Calculations’ or ‘Benchmarks’, storing the corresponding database objects. Objects fields, or database columns, can store strings, text, integers, real numbers or relationship to other objects, with one-to-many and many-to-many paradigms depending on the context. Object data is presented on a dynamically generated HTML page where different fields are displayed and, once logged in, users are granted access to an edition mode. Database items can be modified by the user who created them, and the ***cemff*** administrators. This scheme is chosen to prevent accidental modification of important information and preserve the integrity of the database during its evolution. In the hope of

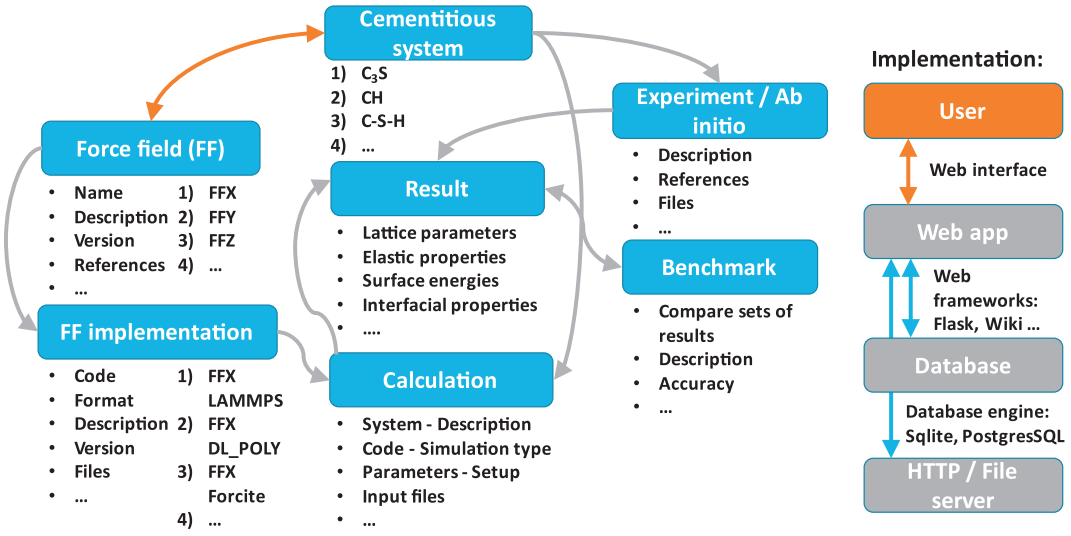

Fig. 1. Schematic of ***cemff*** database structure which includes different types of force field models available for cementitious materials. Text boxes with blue color show the input and comparison sections. (For interpretation of the references to color in this figure legend, the reader is referred to the web version of this article.)

increasing interaction between researchers using the database, an online web forum is included with the interface. Future iterations of the database might add a ranking mechanism where users can rate force fields, according to their own in-situ experience.

The database is structured in a way that it is general enough to accommodate most numerical cases where a force field is involved. A 'forcefield' object is characterized by a name, an author's field, a textual description and a list of 'potential terms'. 'Potential terms' come with a name and a mathematical description, representing the general form of an interaction between two or more bodies. A 'potential term' is expected to have a number of free parameters, while a 'forcefield' is thought of as several 'potential term' items with a definite value for each of the free parameters. At the time of writing, there is no implemented mechanism of making these parameters explicit in the database. In addition, there is the possibility to upload files (simulation code, input files, output files, molecular structures in Cartesian atomic coordinates), add references to scientific articles, as well as references to other force fields and links to possible equivalent versions on the other force field online libraries such as OpenKIM [68] and NIST [69]. Finally, the web application provides a powerful tool that allows a visual comparison of the parameters, corresponding to an arbitrary selection of force-field based calculations and benchmarks, as presented later in Section 3.

2.1. ClayFF force field

As it is clear from the name itself, ClayFF was originally developed in response to a strong need for a robust and flexible force field for molecular simulations of mineral/water interfaces, most particularly – clays and clay-related phases, including metal (oxy-)hydroxides and layered double hydroxides (LDHs) [44]. Computational molecular modeling of such interfaces is especially challenging, because their solid mineral substrate is often incompletely or poorly characterized both in terms of their crystal structure and composition. They often have large unit cells, low symmetry, and large variable composition, and frequently occur as only micron to sub-micron size particles. Obviously, the same compositional and structural complications are typical of most cementitious materials, therefore this force field was almost immediately applied for molecular simulations of several cement-related phases [43,48,74–76].

There are two ways to introduce realistically the necessary mobility and flexibility of such complex hydrated solid substrates without sacrificing the accuracy of the calculation by a common assumption of an entirely rigid or frozen substrate. One can explicitly introduce a set of bonded interaction terms in addition to commonly used electrostatic and van-der-Waals (vdW) terms of the force field. In this approach, all predominantly covalent bonds must be identified and evaluated for each possible local interatomic coordination [49–51,77,78]. However, the application of this approach to systems with complex covalent bond structures may be problematic due to lack of experimental data to constrain all the parameters necessary for a full description of the bonded interactions [79]. The force field parameters must remain thermodynamically consistent, i.e., reproduce structures and surface energies, to be readily transferable among models and simulations [44,51,77]. The overall structure of the force field parameterization must be simple enough to allow modeling of highly disordered systems containing large numbers of atoms and to effectively capture their complex and often cooperative behavior.

Thus, in the development of ClayFF the following arguments were considered. The parameters of octahedrally coordinated Ca in the portlandite structure can be accurately determined with all the necessary bonds, angles, and torsional terms, based on the well-defined X-ray diffraction and other experimental data for $Ca(OH)_2$ crystals. However, this parameterization would hardly be directly transferable for Ca in the structure of tobermorite minerals or Ca in the AFm phase (hydrocalumite), where Ca octahedra are highly distorted. Therefore, the equilibrium bond distances, angles, and torsions are completely different and should be reparametrized in order to properly describe these structures. In view of the above argumentation, the development of ClayFF was based on an alternative approach: to treat the majority of bonded interactions in the crystals as pseudo-ionic (i.e., formally non-bonded), and require that the proper crystal structures and local atomic coordinations are maintained solely by a careful balance between interatomic electrostatic attractions and vdW repulsion terms of the force field [44]. This greatly simplified approach requires dramatically smaller number of force field parameters for its implementation, but allows for molecular simulations of even highly disordered and complex systems containing hundreds of thousands or even millions of atoms. However, one has to remember that it does neglect the nature of chemical bonding which is predominantly covalent and only partially ionic for most silicates [64].

Historically, it is exactly the complexity of the AFm hydrocalumite structure that was an inspiration for the development of this ClayFF-like pseudo-ionic approach to create a force field that ignores explicit definition of bonds and angles [79]. The total potential energy of a simulated system in ClayFF is generally represented by a sum of all

electrostatic interactions, short-range non-bonded (vdW) interactions, a very limited number of explicit bonded interactions:

$$E_{Total} = E_{Coul} + E_{VDW} + E_{Bond\ Stretch} + E_{Angle\ Bend} \quad (1)$$

Electrostatic and vdW interactions are excluded between bonded atoms, and bonds are usually represented by simple harmonic terms. The energy of electrostatic interactions is inversely proportional to the distance between the charges, r_{ij} as described by the Coulomb law:

$$E_{Coul} = \frac{e^2}{4\pi\varepsilon_o} \sum_{i \neq j} \frac{q_i q_j}{r_{ij}} \quad (2)$$

where q_i and q_j are the atomic partial charges, e is the charge of the electron, and ε_o is the dielectric permittivity of vacuum. The vdW term includes the short-range repulsion dominating the increase in energy as two atoms closely approach each other and the attractive dispersion energy at larger interatomic distances:

$$E_{VDW} = \sum_{i \neq j} D_{0,ij} \left[\left(\frac{R_{0,ij}}{r_{ij}} \right)^{12} - 2 \left(\frac{R_{0,ij}}{r_{ij}} \right)^{6} \right] \quad (3)$$

where $D_{0,ij}$ and $R_{0,ij}$ are empirical parameters derived from the fitting of the model to observed structural and physical property data. $D_{0,ij}$ and $R_{0,ij}$, and the partial atomic charges are the key parameters in ClayFF. The vdW parameters between the unlike atoms are calculated according to the arithmetic mean rule for the distance parameter, R_0, and the geometric mean rule for the energetic parameter, D_0:

$$R_{0,ij} = (R_{0,i} + R_{0,j})/2 \quad (4)$$

$$D_{0,ij} = \sqrt{D_{0,i} D_{0,j}} \quad (5)$$

The empirical parameters in ClayFF were originally optimized to accurately reproduce the experimentally known crystal structures of simple and well-characterized oxides, hydroxides, and oxyhydroxides, such as brucite, portlandite, quartz, kaolinite [44]. In this approach, the individual atoms do not have their full formal charges, but rather carry so-called partial atomic charges which empirically account for electron transfer in actual covalent bonds. Oxygen atoms, for instance, typically have partial charges of −0.8 to −1.1, rather than their formal value of −2. These partial atomic charges were derived by Mulliken and ESP analysis from periodic density functional theory (DFT) quantum chemical calculations. Together with the vdW parameters, they were empirically optimized based on the experimental crystal structure refinements of the above model phases. Oxygen and hydroxyl charges vary depending on their occurrence in water molecules, hydroxyl groups, and bridging and substitution environments.

Explicit bonded interactions are used to describe only the O—H bonding in water molecules and hydroxyl groups, and the covalent bonding in polyatomic dissolved species such as sulfate [48] or uranyl [80]. In these cases, the bond stretching (e.g., O—H) and bond angle bending (e.g., H—O—H) interactions are simplified to include only harmonic terms:

$$E_{\text{Bond Stretch } ij} = k_1 (r_{ij} - r_o)^2 \quad (6)$$

$$E_{\text{Angle Bend } ijk} = k_2 (\theta_{ijk} - \theta_o)^2 \quad (7)$$

where k_1 and k_2 are the harmonic force constants. r_0 and θ_0 denote the equilibrium values of the bond length and bond angle respectively.

For water molecules, the flexible version of the simple point charge (SPC) potential was originally used [81,82], and the force field parameters for aqueous cations and anions are largely incorporated from published intermolecular functions compatible with the SPC water model.

Another important general simplification of ClayFF was that for consistency with the SPC water model, the vdW terms centered on all types of O atoms in crystal structures were assumed to be equal to those of the SPC water oxygen, while those centered on the H atoms of structural O—H groups were ignored [44]. The charges on the O and H atoms can vary due to their occurrence in H_2O molecules, hydroxyl groups, and bridging sites. They also vary with nearest neighbor cation substitution in the crystal structures. Thus, ClayFF empirically accounts for charge delocalization due to cation substitution (e.g., Al for Si, or Ca for Al) such that charge is removed from the cationic center to neighboring oxygen depending on the local oxygen environment.

2.2. INTERFACE force field (IFF)

Development of the INTERFACE force field (IFF) began in 2003 and continues today [49–51,77,78,83–85]. IFF is the first uniform classical simulation platform for the assembly of inorganic, organic, and biological nanostructures at the 1–1000 nm scale [51]. It is based on thermodynamic consistency of classical Hamiltonians for organic and inorganic components. The INTERFACE force field parameterizations have been validated for multiple potential energy expressions including the PCFF [86–88], COMPASS [89], CHARMM [90], AMBER [91], GROMACS [92], and OPLS-AA [93] by employing the same functional form and combination rules to enable simulations of inorganic-organic and inorganic-biomolecular interfaces. IFF parameterization emphasizes chemically meaningful atomic charges and van-der-Waals parameters with thorough validation by measured atomic-scale and surface properties [64,77,83,85,94]. The reason is twofold: (1) chemical bonding is reproduced by a chemically realistic balance of covalent versus ionic bonding, which enables also reactive extensions [64], (2) it fulfils the requirement of an accurate quantum mechanical Hamiltonian that reproduces structures (X-ray data) and energies (e.g. surface energy), and energy derivatives (elastic constants, thermal properties). Development of force field parameters requires foremost the analysis of chemical bonding, then the validation of structural and energetic properties that need to be consistent with experimental data (Fig. 2) [51]. It includes rigorous assessment of structural, interfacial, mechanical, and thermal properties of inorganic minerals for establishing the reliability of atomistic force field models and computation of such important properties under various processing conditions. Typically, the validation of structure and energy is sufficient for all other quantities to follow without further adjustments. The atomistic model based on IFF parameters provides a wide range of properties such as lattice constants, densities, surface energies, solid − water interface tensions, anisotropies of interfacial energies of different crystal facets, structural properties (IR and Raman spectra), thermal and elastic constants [49–51,84,85,94].

IFF uses two representative expressions for the total potential energy of a simulated system for classical molecular simulations. The two types of potential energy expressions were chosen to achieve broad applicability of force field parameterization including PCFF [86–88], MMFF [95], COMPASS [89], (using Eq. (8)), and CVFF [96], OPLS-AA [93], AMBER [91], CHARMM [90] (using Eq. (9)). The total potential energy (E_{pot}) (Eqs. (8) and (9)) of the system is the sum of the energy contributions for quadratic bond stretching (E_{bonds}), quadratic angle bending (E_{angles}), as well as electrostatic ($E_{Coulomb}$) and van-der-Waals interactions (E_{vdW}) between atoms and as such depends only on the Cartesian coordinates of the atoms along the directions of the three coordinate axes. The latter two terms, the electrostatic interactions and the van-der-Waals interactions, represent non-bonded interactions. Parameters r_0, θ_0, K_r, K_θ, ε, and σ represent equilibrium bond lengths, equilibrium bond angles, vibrational constants for bond stretching, vibrational constants for angle bending, equilibrium non-bonded energy and equilibrium non-bonded distance between two atoms of the same type, respectively. In mixtures with other elements or compounds, the parameters ε_{ij} and σ_{ij} for non-bonded interactions between different atom types i and j can be obtained by standard combination rules of the respective force field. Further details on the above mentioned parameters as well as combination rules used in the Eqs. (8) and (9) can be found in the elsewhere [51]. The expressions of quadratic bond

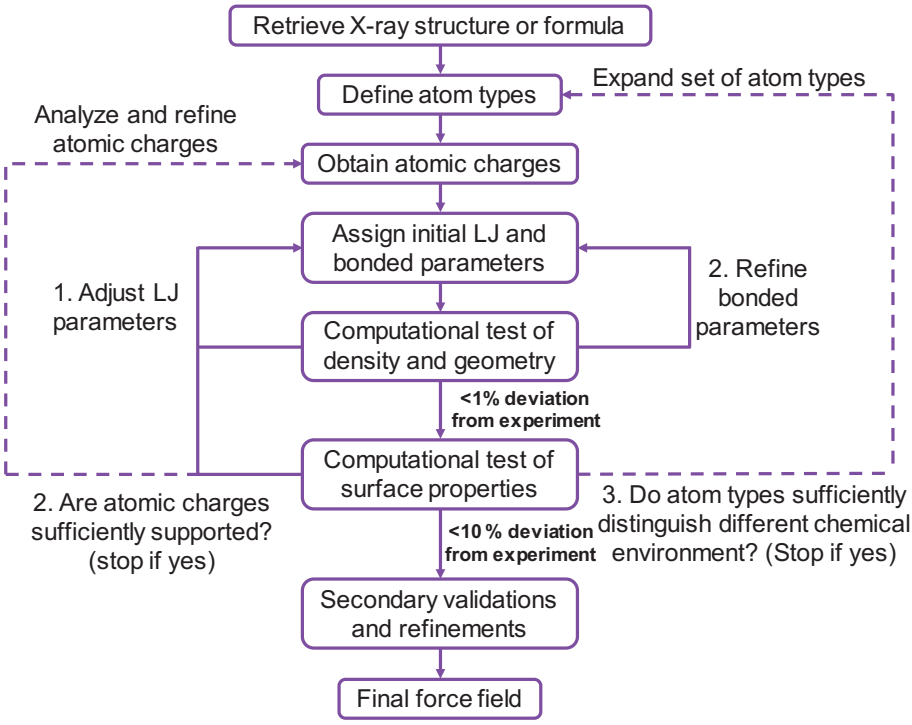

Fig. 2. Procedure for parameterization of new compounds in the IFF, including the most common refinement loops. Careful assignments in every step of algorithm in full agreement with physical and chemical understanding minimize the need for loops. In principle, it is possible to go back to any prior step at each stage in the procedure until thermodynamic consistency is achieved.
Adapted from [ref 51].

stretching (E_{bonds}), quadratic angle bending (E_{angles}) and electrostatic ($E_{Coulomb}$) interactions are same in both Eqs. 8 and 9.

In contrast to other force fields, IFF does not rely on quantum mechanical calculations of atomic charges, as atomic charges obtained from any quantum chemical calculation subject to large uncertainties [64,97]. The charges in IFF reproduce dipole moments and internal multipole moments that have been measured unequivocally in experiment for many compounds. In the approximation of atom-based charges, as used in the force field, the corresponding atomic charges are then exactly defined, i.e., one dipole moment only allows one exact charge distribution. This definition avoids the large uncertainty (up to several 100%) associated with quantum mechanical electron densities and population analysis. For complex silicates and aluminates, the use of dipole moments and related experimental data (deformation electron densities and near-spherical partitions) is complemented by the extended Born model that uses atomization energies, ionization energies, and coordination numbers to further identify relative atomic charges of chemically similar compounds (e.g., known charges for carbon in tetrahedral oxygen coordination in relation to silicon in tetrahedral oxygen coordination, or aluminum in octahedral oxygen coordination relative to calcium and silicon in octahedral oxygen coordination) [47,49,64,77,85,94]. Using multiple independent approaches for each compound to assign the atomic charges, they converge to within < 10% uncertainty and leads not only to consistent atomic charges, but also a reasonable semi-quantitative description of the balance of polar versus covalent bonding that helps in modeling of chemical reactions.

$$E_{pot} = \sum_{ij\ bonded} K_{r,ij}(r_{ij} - r_{0,ij})^2 + \sum_{ijk\ bonded} K_{\theta,ijk}(\theta_{ijk} - \theta_{0,ijk})^2 + \frac{1}{4\pi\varepsilon_0} \sum_{\substack{ij\ nonbonded \\ (1,3\ excl)}} \frac{q_i q_j}{r_{ij}} + \sum_{\substack{ij\ nonbonded \\ (1,3\ excl)}} \varepsilon_{ij}\left[2\left(\frac{\sigma_{ij}}{r_{ij}}\right)^9 - 3\left(\frac{\sigma_{ij}}{r_{ij}}\right)^6\right] \quad (8)$$

$$E_{pot} = E_{bonds} + E_{angles} + E_{Coulomb} + \sum_{\substack{ij\ nonbonded \\ (1,3\ excl)}} \varepsilon_{ij}\left[\left(\frac{\sigma_{ij}}{r_{ij}}\right)^{12} - 2\left(\frac{\sigma_{ij}}{r_{ij}}\right)^6\right] \quad (9)$$

Presently the IFF database includes validated models of clay minerals, fcc metals, silica, comprehensive coverage of cement minerals, calcium sulfates, hydroxyapatite and poly(ethylene oxide). To understand realistic chemical reaction mechanism in successive steps, it also provides representative surface models with variable surface chemistry and a range of pH values. There are also no adjustable or numerical "fit" parameters as every parameter is grounded in a physical chemical interpretation. Silicate parameters for C-S-H, for example, are consistent with those for silica and clay minerals, and allow quantitative predictions for any water and organic interfaces [84,98]. A limitation is the difficulty to simulate chemical reactions, however, algorithms for bond breaking and formation including experimentally verified and quantum-mechanical criteria can be included for specific chemical reactions [99].

2.3. Cement force field (CementFF)

The salient feature of cement force field is its applicability to all cementitious systems. The force field is developed by combining and adapting potentials developed for systems with similar atomic species. The calcium-oxygen interaction is from the adaptation of Freeman et al. [100] using the formulation of Schroeder et al. [101] on the force field originally developed by Lewis and Catlow [102]. These interactions are based on Buckingham functional forms and the species have full formal charges except for the hydroxyl groups (OH). Additionally, Freeman et al. [102] used TIP3P for the water model and this is replaced by TIP4P/2005 potential developed by Abascal and Vega [103] which gives better agreement to the physical and thermodynamic properties of water.

The work of Freeman et al. did not include systems containing silicates. For the silicon–oxygen and oxygen–oxygen interactions, the potential parameters are adopted from Leeuw and Parker [104,105] which consisted of polarizable oxygen shells. These shells were

removed in accordance with the work of Freeman et al. [100] and this leads to a straightening of the Si–O–Si angle. In order to correct this, a Si—O—Si harmonic angle potential was introduced and the parameters were chosen to fit the experimentally observed Si—O—Si angle in quartz. An additional harmonic angle potential describing Si—O—H angle was also added to the force field. Except for water and hydroxyl, all other atoms have full formal charges. This has the big advantage that no special care has to be taken to model defects, such as surfaces, where partial charges might change as well as the adsorption of ions from the solution. It has been said, that a full atomic charge force field leads to excessive restructuring and water density fluctuations at solid-water interfaces. However, comparison between water density fluctuations at the (0 0 1) surface as calculated with the current and the partial atomic charge used in ClayFF force field [48,75] does not show any indication of such excessive restructuring [106]. The full parameters of the force field can be found in the supporting information of previous publications [66,67].

The resulting force field has been tested on lime, portlandite, alite (triclinic crystal), quartz, tobermorite 9 Å and tobermorite 14 Å [106,107]. The ability of the force field to simulate the structure of solvated calcium and hydroxyl ions are also used to validate the applicability to cementitious systems. As an additional validation, the reaction enthalpies of several chemical reactions, involving the above mentioned minerals/phases and different aqueous species, have been calculated and which were found to be in good agreement with experimental values [106,107]. Based on these values empirical expressions for the estimated errors on structures and enthalpies have been developed [106,107].

2.4. ReaxFF force field

ReaxFF is a reactive force field initially developed by A.C.T van Duin and coworkers to investigate the combustion reactions [62] and was rapidly adapted to the investigation of inorganic materials [108]. In ReaxFF the potential energy of the system E_{total} is computed from the expression:

$$E_{total} = E_{bond} + E_{angle} + E_{torsion} + E_{over} + E_{vdWaals} + E_{Coulomb} + E_{specific} \quad (10)$$

The first four terms ($E_{bond} + E_{angle} + E_{torsion} + E_{over}$) describe the short range interactions between bonded atoms, and correspond to the interatomic two body bonding energy, the three body angular energy, the four body torsion energy, and a penalty energy to avoid over coordination. Unlike traditional force fields, ReaxFF does not use constant functions to relate interatomic distances or angles with the potential energy for the bonding interactions. The potentials are bond-order dependent continuous functions. In short, the bond-order is a quantity that represents the electron density in the region between two atoms [109], hence giving an idea of how strong is the bond between them. At each step of the simulation, the bond-order is computed from the atomic position and introduced into the potentials, balancing the interaction. If the bond-order between two atoms decreases, so does the interaction energy, until it goes to zero, when effectively the bond between them breaks. The next two terms ($E_{vdWaals}$ and $E_{Coulomb}$), represent the non-bonded van der Waals and Coulomb energies, and the last term, $E_{specific}$ includes specific energy terms for certain systems, like hydrogen bonding and lone pairs in water molecules, or conjugation in hydrocarbons. The Columbic energy is a long range interaction due to atomic charges. In ReaxFF, atomic charges are computed at each simulation step by an electronegativity equalization method (EEM) [110,111]. This allows the description of polarization effects of molecules in different environments. Finally, a key characteristic of the ReaxFF formalism, necessary to accomplish chemical reactions, is the fact that each atom has a unique identity. For instance, there is a single type of oxygen atom, whether it is part of a water molecule, tricalcium silicate, or the C-S-H gel, and it will be able to migrate from one type to another if chemical reactions take place. This is a notable difference with non-reactive force fields where an atom can have different "identities" depending on the chemical environment, i.e. water oxygen is different from silicate oxygen, they are not exchangeable, and each of them has a particular set of empirical parameters and atomic charge.

In practice, the ReaxFF formalism translates into a great flexibility to describe molecular properties, but more importantly, ReaxFF makes it possible to simulate chemical reactions and determine transition states accurately [112,113]. This allows the simulation of chemical reactions in considerably larger systems with respect to DFT or semi-empirical methods [114]. ReaxFF has been widely employed to study catalysis [115,116], material failure [117], gas-phase reactions [118] and aqueous phase chemistry [119]. For more information about the methodology details, the applications, and the implementation and acceleration possibilities, we suggest the reader refers to some recent reviews [120,121].

ReaxFF application to cement research was facilitated after the parameterization of the Ca/O/H set by Manzano et al. [45]. This set was merged with the existing Si/OH/set [122], making the full Si/Ca/O/H set available to study the most relevant phases of cement, calcium silicates and their hydration products [123]. Since then, considerable research has been conducted to determine the correlation between the C-S-H structure (water content, silicate chain length, Ca/Si ratio, and order-disorder) and properties [33,124–128], with special focus on mechanics and confined water dynamics [35,45,129,130]. Besides calcium silicate hydrates, the Ca/O/H set was also used by Liu et al. to investigate mechanical failure of ettringite [40], a work that showed the potential transferability of the Ca/O/H set of parameters to study other oxides, incorporating for instance sulfate groups and/or aluminum atoms [131]. A second area of interest is the dissolution of cement minerals, which will be addressed in detail in Section 5.

2.5. CSH-FF force field

CSH-FF is a force field potential developed for hydrated calcium-silicates [132] using both structural and elasticity data [43]. It is an improved version of the core-only model ClayFF [44] because it is designed for predicting both structural data and high-order properties (i.e. elastic constants). Compared to other force fields such as core–shell potentials [133] and ReaxFF [62], CSH-FF is less expensive computationally and thus more efficient for larger systems.

The CSH-FF predictive capabilities are rigorously benchmarked against first principles results for two tobermorite polymorphs distinguished by their basal spacing and hence water content: 14 Å tobermorite [134] and 11 Å tobermorite [135]. Note that tobermorite polymorphs also differ in chemistry in terms of Ca/Si ratio: the 14 Å tobermorite by Merlino has a Ca/Si ratio equal to 0.83; while 11 Å tobermorite by Hamid has Ca/Si ratio ranging from 0.67 to 1, among which the one of ratio equal to 1 is employed [135]. Since ClayFF was designed for predicting structural data, it has some shortcomings in predicting higher order properties such as elastic constants. The limited degree of transferability of ClayFF for complex hydrated calcium-silicate materials requires an improvement of the second-order predictive capabilities [136].

An inspiration for such an improvement comes from SiO_2 core-only potentials that give a good account of many properties of quartz including structural and elasticity properties [137]. These potentials are based on the same set of equations as ClayFF but use different parameters. It should be noted that some of the partial atomic charges used in the ClayFF model, are different to those derived for the C-S-H FF using quantum calculations. The atomic charges are significantly different than those derived from the reference DFT calculations [138].

In the spirit of the core-shell approach, short-range Lennard Jones interactions between cations are not considered in CSH-FF, and the cation-cation Coulombic repulsion are assumed to be sufficient, leading to a simpler description as compared to ClayFF. All fitting and

parameterization of the CSH-FF potential were performed using the GULP code [61].

From the quantum-derived charges, there is a distinction between calcium atoms in different chemical environments e.g. interlayer calcium (C_w), and intralayer calcium (Ca). Unlike the atomic charge of calcium ion used previously in ClayFF. CSH-FF uses as a set of fitting data from extensive DFT calculations including the cell parameters, the bulk and shear moduli and the entire 21 elastic constants of tobermorite 11 Å; thus in total 29 input data. During fitting, all short range (Lennard-Jones) parameters (except the non-bonded interactions between C_w and O, O_w and Ca, O_w and Si parameters are selected from ClayFF initial values as they are found to have no significant energy contribution) were freely adjusted with respect to the DFT data. In brief, CSH-FF is derived based on fitting 29 parameters (Lennards-Jones parameters + atomic charges) to 29 observable input data with equal weight. More detailed information on the fitting procedure can be found in ref. [43]. The parameters for CSH-FF are given in Tables S4 and S5.

3. Model validations

This section deals with the comparison of experimental and computed data on structural, mechanical and surface properties of representative cementitious phases. The validation of each mineral is described in this section along with force field parameters mentioned in the supporting information and in the ***cemff*** database. Contributions towards validated atomistic models have been reported by five research groups involved in the atomistic force field development for cement as well as other inorganic minerals. Lattice parameters, mechanical properties, surface as well as interfacial energies of portlandite (CH), tricalcium silicate (C_3S) and tobermorite (model C-S-H) minerals (Fig. 3) using different force fields have been included (Table 1, Table 2 and Table 3). We present a detailed description on model validations by each force field in a separate subsection. A comparative analysis and further discussion on presented force fields have been provided in Section 4.

3.1. Model validations using ClayFF

Over the last 10–15 years, ClayFF has been successfully tested in numerous molecular simulations of a wide range of systems, showing good promise to further evolve into an adaptable and broadly effective force field for molecular simulations of clays, cement phases [139,140] and other aluminosilicate materials and their interfaces with aqueous solutions [44,48,75,141–143]. Table 1 and Table S1 illustrate that, despite its simplicity, ClayFF is able to quite accurately reproduce the crystallographic parameters of many cement-related phases. The good agreement for portlandite is, of course, not surprising, because its crystal structure was initially used to fit the force field parameters. However, all other structures in Table S1 were simply constructed out of a relatively small number of originally parameterized "building blocks", assuming their transferability within the ClayFF modeling approach. ClayFF can be implemented into the most common molecular simulation packages such as LAMMPS [144], GULP [61], DL_POLY [145], NAMD [146] and TOWHEE [147].

In addition to structural properties, ClayFF quite accurately reproduces the energetics of swelling for a wide range of layered silicates and hydroxides [75,143,148]. In particular, the MD-simulated energetics of water sorption in Na- and K- kanemite, [(Na, K) $HSi_2O_5{\cdot}nH_2O$], is found to be in excellent agreement with the observed X-ray diffraction, water sorption, TGA/DTA, and ^{29}Si NMR data [142]. Kanemite-like volumes appear to be a significant component of alkali silicate hydrate (A-S-H) gels with compositions in the range observed for in-service concrete. XRD data suggest that these nano-particles are 10–20 nm thick perpendicular to the silicate layers. MD modeling has shown that entry of water into the interlayer spaces of kanemite is structurally and energetically limited and, thus, that expansion of the alkali silicate hydrate (A-S-H) gels produced during the alkali silica reaction (ASR) is due to incorporation of water molecules principally between nano-particles, rather than within kanemite-like interlayer

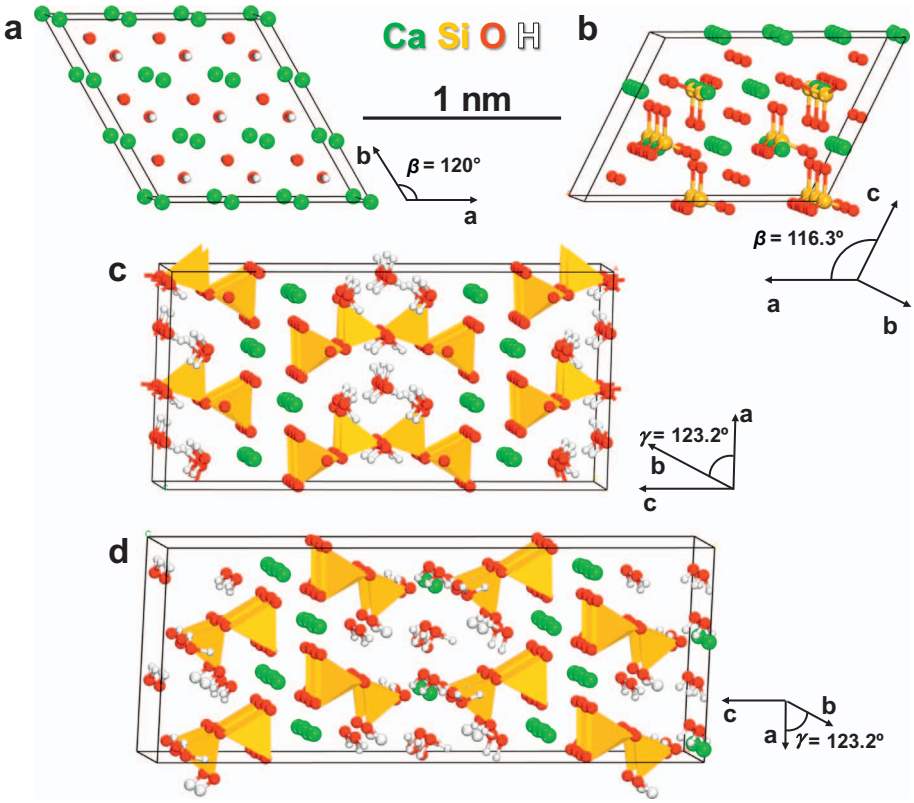

Fig. 3. Crystal structures of selected cement minerals are shown. (a) portlandite (trigonal crystal system) [ref 152], (b) M_3 polymorph of tricalcium silicate (monoclinic crystal) [ref 151], (c) tobermorite 11 Å [ref 153] and (d) tobermorite 14 Å (monoclinic crystal) [ref 134]. Lattice constants from XRD data are also presented in Table 1 for all minerals.

Table 1
Lattice parameters of cementitious mineral crystals according to experiment and NPT molecular dynamics simulation using various force field types under standard temperature and pressure.

Mineral	Force field type	Method	Cell dim.	*a* (nm)	*b* (nm)	*c* (nm)	*α* (°)	*β* (°)	γ (°)	*V* (nm^3)	ρ (g/cm^3)	% Error
Portlandite (trigonal)		Experiment [152]	1 × 1 × 1	0.3589	0.3589	0.4911	90	90	120	0.0548	2.246	0
	DFT [158]	EM[b]	1 × 1 × 1	0.369	0.369	0.497	90	90	120	0.0586	2.10	6.48
	ClayFF [44]	MD	1 × 1 × 1	0.357	0.357	0.491	90	90	120	0.0542	2.27	1.09
	IFF[a]	MD	1 × 1 × 1	0.375	0.375	0.438	90	90	120	0.0533	2.30	2.74
	CementFF [46]	MD	1 × 1 × 1	0.368	0.367	0.481	90	90	120	0.0564	2.18	2.92
	ReaxFF [45]	EM	1 × 1 × 1	0.366	0.366	0.486	90	90	120	0.0564	2.18	2.92
Tricalcium silicate (monoclinic)		Experiment [151]	1 × 1 × 1	1.2235	0.7073	0.9298	90	116.31	90	0.7213	3.154	0
	IFF [49]	MD	1 × 1 × 1	1.224	0.704	0.934	90	116.2	90	0.7230	3.15	0.23
	CementFF	MD	1 × 1 × 1	1.243	0.719	0.957	89.7	115.6	90	0.7710	2.98	6.93
	ReaxFF [58]	EM	1 × 1 × 1	1.217	0.708	0.933	90	117.2	90	0.7150	3.18	0.87
Tobermorite-11 Å (monoclinic)		Experiment [153]	1 × 1 × 1	0.6735	0.7385	2.2487	90	90	123.25	0.9354	2.460	0
	DFT [138]	EM	1 × 1 × 1	0.660	0.740	2.313	90	90	123.6	0.9407	2.45	0.57
	ClayFF	MD	1 × 1 × 1	0.677	0.733	2.451	91.1	90	123.1	1.0145	2.27	8.45
	IFF	MD	1 × 1 × 1	0.685	0.737	2.257	90	90	122.5	0.9605	2.40	2.68
	CementFF	EM	1 × 1 × 1	0.687	0.729	2.348	90	88.3	121.8	0.9988	2.30	6.78
	ReaxFF	EM	1 × 1 × 1	0.681	0.765	2.308	90	90	123.9	0.9981	2.31	6.70
	CSH-FF [43]	EM	1 × 1 × 1	0.66	0.739	2.437	90	90	123.88	0.9958	2.31	6.45
Tobermorite-14 Å (monoclinic)		Experiment [134]	1 × 1 × 1	0.6735	0.7425	2.7987	90	90	123.25	1.1704	2.227	0
	DFT [138][c]	EM	1 × 1 × 1	0.687	0.743	2.849	90	90.1	123.47	1.2131	2.15	3.65
	ClayFF	MD	1 × 1 × 1	0.687	0.737	2.855	89.2	90	122.69	1.2164	2.14	3.93
	IFF [51]	MD	1 × 1 × 1	0.677	0.735	2.785	90	90	122.55	1.1673	2.23	0.26
	CementFF	MD	1 × 1 × 1	0.686	0.727	2.741	88	91	123	1.1520	2.27	1.57
	ReaxFF [33]	EM	1 × 1 × 1	0.668	0.750	2.833	91.1	89.4	124.32	1.1720	2.22	0.14
	CSH-FF [43]	EM	1 × 1 × 1	0.67	0.741	2.870	90	89.8	123.77	1.1909	2.19	1.75

[a] Reproduction of lattice parameters has been done using supercell of ~(1.5 × 1.5 × 1.5 nm^3). Parameters have been normalized to make it compatible to compare with others simulated data and unit cell parameters from X-ray data.

[b] Using energy minimization (EM) or DFT method, lattice parameters are reproduced at 0 K, while the X-ray data measured under ambient condition as a benchmark. The current data from energy minimization at 0 K need to be followed with MD simulations for a more quantitative comparison. MD simulation using NPT ensemble at 298 K provides more quantitative comparison.

[c] Calculation from reference [139] was performed by Density Functional Theory (DFT) using GGA exchange correlation functionals. For energy and stress calculations, ultrasoft pseudopotentials with a plane wave basis set and a cutoff energy of 420 eV for the wave functions and 50,350 eV for the charge density were used.

galleries [142]. The ClayFF-optimized structures of Na- and K-kanemite are in excellent agreement with those determined from X-ray diffraction data (Table S1).

3.2. Validations of atomistic models using IFF

Interpretations of IFF parameterization for inorganic minerals are well discussed in Section 2.2. It is very important to establish the reliability of these atomistic force field models used for cementitious systems. This has been achieved by reproducing the cell parameters (Table 1), mechanical properties (Table 2), surface and interfacial energies (Table 3) of the atomistic models in comparison with available experimental data. In general, IFF follows a rigorous validation scheme that includes vibrational spectra (IR and Raman), heat of immersion, thermal expansion coefficient, and a full range of surface ionization data corresponding to pH in addition to the above mentioned properties

Table 2
Mechanical properties of cementitious minerals from available experimental data and molecular simulations using NPT molecular dynamics.

Mineral	Method/force field type	Bulk modulus *K* (GPa)	Shear modulus *G* (GPa)	Poisson's ratio *ν*	Young's modulus *E* (GPa)		
					E_x	E_y	E_z
Portlandite	Experiment [159–161]	40 ± 7	16 ± 3	0.32 ± 0.02	*E* = 43 ± 8		
	CementFF	34	21	0.24	53		
	IFF	41 ± 5		0.35 ± 0.04	83 ± 3	83 ± 3	49 ± 2
	ReaxFF [45]	45	21	0.30	63	63	17
Tricalcium silicate	Experiment [161,162]	105	45	0.31	*E* = 118, 143 ± 8		
	IFF [49]	105 ± 5		0.33 ± 0.03	143 ± 8	143 ± 8	103 ± 11
	CementFF	100	49	0.29	127		
	ReaxFF [58]	77	55	0.21	142	138	139
Tobermorite-11 Å (Ca/Si = 0.67)	Experiment [163]	69 ± 5			Not known		
	DFT [138]	67	32	0.30	83		
	IFF	71 ± 2		0.29 ± 0.04	128	134	80
	CementFF	75	32	0.31	84		
	ReaxFF	103	31	0.33	82	92	113
	C-S-H FF [43,135]	60			151	123	61
Tobermorite-14 Å (Ca/Si = 0.83)	Experiment [164]	47 ± 3			Not known		
	DFT [138]	36	21	0.30	52		
	IFF	44 ± 2		0.31 ± 0.04	41	68	24
	CementFF	45	26	0.29	67		
	ReaxFF	44	22	0.29	51	55	36
	CSH-FF [43]	42 ± 2			101	88	57

Table 3
Experimental and theoretical values of surface/cleavage energy, solid-water interfacial energy of cementitious minerals under ambient conditions.

Mineral	Method/FF type	Crystal plane	Surface/cleavage energy, mJ/m^2	Interfacial energy (solid-water), mJ/m^2
Portlandite	Experiment [165–167]	Not known	1180 ± 100	65, 68
	CementFF	(001), ((100)), (((101)))	(100 ± 30), ((600 ± 60)), (((740 ± 100)))	(110 ± 60), ((130 ± 60)), (((90 ± 60)))
Tricalcium silicate ($3CaO{\cdot}SiO_2$)	Experiment [165,168]	Not known	CaO: 1310 ± 200[a]	−870 (C_3S dissolution)
	DFT [156]	(001), ((010)), (((100)))	(1190), ((1090)), (((1380)))	
	IFF [49,85]	Crystal facet average	1300 ± 50	−830 ± 40
	ReaxFF [58]	(001), ((010)), (((100)))	(1310), (1640), (((1460)))	
Tobermorite-11 Å (Ca/Si = 0.67)	Experiment	Not known	Not known	Not known
	IFF	(004), ((100))	(680 ± 20), ((695 ± 20))	
Tobermorite-14 Å (Ca/Si = 0.83)	Experiment [169][b]	Not known	386 ± 20 (Ca/Si = 1.50)	Not known
	IFF	(001), ((100)), (((004)))	(405 ± 10), ((605 ± 20)), (((670 ± 20)))	
	ReaxFF	(001), ((100)), (((010)))	(100), ((850)), (((1200)))	

[a] Experimental value for similar mineral CaO is shown (not known for Ca_3SiO_5).
[b] Experimental value of tobermorite with high Ca/Si ratio is mentioned due to absence of data for low Ca/Si ratio tobermorite. 4. Comparisons of Force Field Models.

[50,83,84,94]. IFF provides validated atomistic model of calcium sulfates, silica, tricalcium aluminate, ettringite, pH-sensitive hydroxylated C_3S surface, tobermorites and monosulfate minerals [50,51,84,85]. These minerals have a very important role during cement hydration. To run the molecular simulations using validated IFF models, one can use the computer simulation packages such as LAMMPS [144], Material Studio [149], GROMACS [150], NAMD [146] and TOWHEE [147].

Models of three-dimensional periodic super-cells of portlandite, tricalcium silicate, tobermorite 11 Å and 14 Å were built using the known X-ray diffraction data [134,151–153]. Details of the construction of models are fully described in our earlier papers [49,51]. Different sizes of simulation boxes were used for the reproduction of cell parameters, bulk modulus, Young's modulus, surface as well as interfacial energy. We emphasize that the simulation results are independent of box size as long as dimensions exceed 1.2 nm, i.e., larger than the range of electrostatic interactions (in charge-neutral systems with dipoles < 0.3 nm apart) and van-der-Waals interactions. Minor statistical errors may also occur during the simulations. But it can be avoided by using suitable simulation protocols and good statistics. Computed lattice constants and densities of crystal structures for all compounds listed in Table 1 exhibit very small deviations from X-ray diffraction data, typically as low as 0.2 to 1% using MD simulations under the NPT ensemble. Mechanical properties including bulk modulus, Poisson's ratio and Young's modulus of all compounds deviate 0 to 10% from experiment (Table 2). The solid-vapor and solid-liquid interfacial energies for different crystal facets deviate 0 to 10% from experiment for inorganic compounds (Table 3). Overall, IFF reproduces a wide range of physical, chemical, mechanical and thermal properties in quantitative agreement with experimental measurements [51]. In this paper, we have presented revised force field parameters of tobermorite minerals (mentioned in the supporting information, Table S2). Improvements of the tobermorites and C-S-H force field models are still subject to ongoing research.

3.3. Model validations using CementFF

Classical molecular dynamics using DL_POLY code [145] with a time step of 0.7 fs, Ewald summation for long range forces and a cut off of 8.5 Å has been used for all the systems reported here. Portlandite has been thoroughly studied using this force field [106,154]. As shown Table 1, the force field is able to capture the lattice parameters within the estimated error of 5% on bond distance. The elastic properties were derived from the elastic tensor, using the Hill definition for the bulk and shear moduli calculated with METADISE package (Table 2) [105]. The calculated properties are either within or just outside the error limit of the experimental values as can be seen in Table 2. Cleavage energies calculated using METADISE package and the water-portlandite interfacial energies for different crystallographic surfaces are shown in Table 3 [46]. CementFF can be easily implemented in most of the molecular dynamics packages such as LAMMPS [144], GULP [61] and DL_POLY [145].

3.4. Validations of atomistic models using ReaxFF

The structure and elasticity of the test systems (Table 1 and Table 2) were computed by energy minimization. A $3\times3\times3$ supercell of tricalcium silicate (C_3S) was studied with the help of LAMMPS program [144] using a conjugate gradient minimization algorithm with energy and force tolerance cut-offs of 10^{-5} kcal/mol. The elastic tensor coefficients were obtained from the stress-strain linear fits, applying strain from +3% to −3% (expansion and compression respectively) in steps of 0.5% for all the strain matrix elements. Portlandite and tobermorite were simulated with the help of GULP [61] using a $2\times2\times2$ supercell for the former and $2\times2\times1$ for the later. The energy minimizations were done using a Newton-Raphson algorithm, and the elastic tensor coefficients were determined by the internal routines of GULP from the second derivatives of the energy respect to the applied strain. The elastic properties of all the phases were derived from the elastic tensor coefficients, using the Hill definition for the bulk and shear moduli [155]. Surface energies of tricalcium silicate and tobermorite were computed using molecular dynamics simulations. For both systems, we built slabs of thickness 3 nm and cross-sectional area of 2 nm^2 with 3 nm vacuum space to avoid self-interactions, the computed surface energies of minerals were presented in Table 3 [156]. Since ReaxFF uses particular functional forms (Eq. 10), it cannot be used directly in any simulation code. The main codes with ReaxFF implementations are GULP [61], LAMMPS [144] and PuReMD [157].

3.5. Validations of atomistic models using CSH-FF

The rigorous validation of CSH-FF has been achieved for two cases (the 11 Å tobermorite, and the 14 Å tobermorite) where the 11 Å tobermorite has been used for the development of CSH-FF parameters, but the 14 Å tobermorite has not [52]. Note that the atomic charges in CSH-FF are significantly different from both DFT and ClayFF atomic charges except for water (unchanged during fitting) (see Table S4). Therefore, they should be considered as effective potential fitting parameters. The quality of the fitting can be seen in the good agreement for tobermorite 11 Å, in both structural data (Table 1), and elasticity data (see Tables 2, S6, S7 and S8). The comparisons of the elastic tensor are not only for each component, but also for three other measurements of the elastic tensor: Euclidean distance, Riemannian metric, and Voigt–Reuss–Hill (VRH) approximation (See S1.5). The good agreement for 11 Å tobermorite is self-evident because the fitting process is based on this crystal structure. As a further validation, 14 Å tobermorite (Table 1) and its elasticity data (Tables 2, S9, S10 and S11) are examined. Interestingly, in some cases CSH-FF displays superior performance than the core–shell model [43] for a significantly smaller

computational effort. Note that for hydroxyl groups (O—H) present in tobermorite 14 Å, CSH-FF uses the same parameters as derived in ClayFF. In this case, to ensure the charge neutrality of the cell, the small extra positive charge is divided between all the cation atoms. In addition, the ability of CSH-FF is also demonstrated for a porous glassy calcium silicate hydrate (C-S-H) model. CSH-FF can be implemented in common molecular dynamics programs like LAMMPS [144], GULP [61], and DL_POLY [145].

4. Comparisons of force field models

In general, force field development which includes the parameterization as well as validation is a scientifically rigorous and labor-intensive effort. For any type of force field model, it is very important to ensure that the computed results are consistent with experimental findings. This begins with the quantitative reproduction of the lattice constants under experimental conditions (Table 1). In the secondary validation step, it has been considered to compare mechanical and surface properties of selected minerals (CH, C_3S and model C-S-H) with available laboratory data (Table 2 and Table 3). To simplify this paper, we have not focused on other important properties such as computation of vibrational constants using IR/Raman spectra, compatibility of parameters with other form of energy expression, thermal properties and phase diagram, etc.

ClayFF and CSH-FF parameters for cementitious minerals have not to date been validated for surface and interfacial properties. The parameters for Ca in the ClayFF for portlandite structure are not applicable for tobermorite minerals or Ca in the AFm phase (hydrocalumite), where Ca octahedra are highly distorted. This can be also seen in the lattice reproduction of tobermorite minerals (Table 1). In this scenario reparametrization of ClayFF parameters for tobermorite and other minerals would be an important step to refine these models for further validations. The assumption of a pseudo-ionic system without covalent contributions to bonding leads to large overestimates in surface, interface, and adsorption energies. In this case atomic charges must then be chosen to be larger to produce an equivalent cohesion [77]. Therefore, self-assembly at mineral surfaces in solution or with organic compounds cannot be consistently simulated.

One principal limitation of ClayFF, as well as any other non-reactive classical force fields such as IFF, CementFF, CSH-FF is that they do not allow us to model ligand exchange reactions. Such as the making and breaking of O—H bonds, thus preventing modeling of proton exchange reactions in the fluid or with the surface, which are extremely important for cementitious systems. This limitation requires the researcher to make a priori decision about the surface protonation state of the model to simulate, for instance, the pH dependent behavior. More rigorous approaches would require the application of computationally very expensive ab initio MD techniques [170], or, at least, application of a “reactive” force field [45]. ReaxFF has limitations with atomic charge calculations as it does not incorporate the polarizable charge transfer model. This has a few drawbacks, (1) inability to restrain long-range charge-transfer between molecular fragments that are well separated and this leads to nonzero charges on isolated molecular species, (2) unrealistic charge-transfer may also occur during simulations of dense systems [120]. Nevertheless, having a variable charge could also lead the way for more realistic charges than fixed charge systems (specially formal atomic charge) in many situations, e.g. solid-liquid interfaces and defect sites. In addition, the ACKS2 charge calculation method, not yet in ReaxFF descriptions for Ca/Si/O/H systems, removes both the non-zero charge and the long-distance charge transfer issues associated with the EEM/Qeq charge transfer concepts [171].

As mentioned earlier, CementFF can be treated as a general force field that can be applied to a variety of cementitious systems with reasonable accuracy. Unlike ClayFF, IFF and CSH-FF, this force field does not have different description of calcium, silicon, hydroxyl and oxygen species (bonded to the silicon) within a system or among different cementitious systems, simplifying the transferability to other $Ca/Si/O/H/H_2O$ systems. Moreover, the system is then not heavily constrained to the different description of a species in different chemical environments. However, with this general description, the errors in the simulated cell parameters reach within 1–10% relative to the experimental values, but the mechanical properties are still estimated in a reasonable range if not as accurate as other force fields.

DFT calculations are typically at least a million times more computationally expensive for the same system size and number of steps in comparison with a classical force field. Specifically, computation times in DFT scale with a power of the number of basis functions, e.g., the number of valence electrons N with $O(N^3)$, and MD with the number of atoms, e.g. $O(N^2)$ or $O(N\ln N)$, which increases the difference in computational cost for larger systems [51]. DFT is also prone to some uncertainties associated with empirical assumptions in density functionals. At the same time, classical approaches, such as ClayFF, CementFF, and IFF have inherent difficulties to model chemical reactions (except, for example, bond breaking). However, the force fields can be applied to simulate the systems at various equilibrium states, e.g., before and after the reaction. Androniuk et al. [26] have recently applied this approach, for ClayFF, to develop a series of classical C-S-H models corresponding to different Ca/Si ratios and different degrees of surface protonation, using experimental ^{29}Si MAS NMR data and accurate quantum chemical results as a guidance [14,170,172]. The models were then applied to simulate adsorption of uranyl and gluconate ions at the hydrated C-S-H surfaces as a function of Ca/Si ratio and solution pH, and to interpret on the molecular scale the experimentally observed behavior of these systems [26].

Although ReaxFF most noticeable feature is the capability of reproducing chemical reactions, the properties computed with ReaxFF match very well with the experimental values and ab-initio simulations, except from an apparent overestimation of tobermorite 11 Å elastic properties. Its accuracy is comparable to the rest of the methods presented in this work, and given its generality and transferability (all the phases can be simulated with the same set of parameters) it could be a good choice to make consistent studies across different phases. The main disadvantage of ReaxFF is its considerable computational cost and lack of validation of surface properties. For instance, ReaxFF simulations are about two orders of magnitude slower than ClayFF, due to the intrinsic formalism and the smaller time step needed for capturing correct dynamics and reactivity. Therefore, despite ReaxFF is the natural choice to investigate chemical reactions, it is recommendable to examine other force fields if they have not already been validated using in ReaxFF simulations.

Specialized energy expressions of intermolecular potentials (Buckingham as well as ReaxFF) are typically more limited in compatibility with other harmonic energy expressions e.g. PCFF, CHARMM, AMBER, COMPASS, GROMACS, and OPLS-AA. In contrast, IFF is compatible with these materials-oriented and biomolecular force fields as it follows a consistent validation of chemical bonding, structures, energies, and energy derivatives for each compound. It allows the simulation of a vast number of new interfaces with water, biomolecules, and polymers without further addition of parameters; computed binding energies are typically within 10% agreement with experimental measurements. Moreover, interfaces between different cement minerals and cement-related minerals (silica, clays, calcium sulfates) are feasible. Compared the other force fields, it achieves the closest match in surface and interfacial properties as it is based on a thorough analysis of atomic charges, coordination environment, and atomic polarizabilities [47]. Changes from Eq. (8) 9–6 LJ potential to Eq. (9) 12–6 LJ potential while maintaining the same atomic charges can lead to differences up to 10% in computed mechanical and thermal properties [51].

Several suggestions have been made to modify the parameters of ClayFF to bring various simulated properties in closer agreement with experimental data [43,173–175]. A systematic work on improvement of the ClayFF parameterization is currently on-going along two important

directions with respect to their future application for cementititous systems: (i) making it fully compatible with more complex and accurate H_2O molecular models in order to improve the accuracy of description of the structural and dynamic behavior of substrate-water interfaces and make it compatible with common force field for organic substances [176]; (ii) the development of additional metal—O—H bending terms (Si—O—H, Al—O—H, etc.) which facilitate the accurate description of inorganic nanoparticle edges, including for instance the edges of C-S-H particles [177].

IFF has an extremely broad applicability to simulate bulk and surface properties, including nanoparticle growth and surface complexation by ligands, which has been demonstrated in a series of publications in agreement with experiment [49–51,77,84,85,98,178]. It is important to use common (hkl) cleavage planes and create electroneutral surfaces, or facets, of nanoparticles [85,94,99,179–181]. Thereby, typically no changes in atomic charges and force field parameters are necessary. Subsequently, the surface chemistry in solution must be represented in accordance with experiment including the correct proportions of SiOH groups versus SiO^- and Ca^{2+} groups, as well as aluminate versus aluminol groups depending on the pH value [84,85]. The IFF surface model database includes sample surface models that indicate appropriate force field types and atomic charges ready to use, as well as literature references with experimental data [51].

Accuracy of the force field is very sensitive to the structural variance. A unique set of force field parameters might not be applicable for all tobermorite minerals due to different Ca/Si ratios, chemical environment for interlayer calcium ions and basal spacing. Although tobermorite 11 and 14 Å have similar layered feature, simulated results with minor deviations can be seen in the case of tobermorite minerals (Tables 1 and 2). This happens because only one unique set of all-atom force field for tobermorite 11 and 14 Å were developed by each force field group. Each type of tobermorite may require unique set of force field parameters to get a very good match in comparison to experiment. Individual set of force field for each tobermorite type would complicate the steps of atomistic modeling specially during the simulations of phase change phenomena and hydration studies. That's why each force field group used a unique set of force field parameters, which could be applied for all tobermorite minerals with minimum deviation and simultaneously consistent with experiment.

5. Applications of force field models

5.1. Application of ClayFF to study calcium silicates hydration

For quantitative understanding and prediction of the mechanical and chemical properties of hydrated cement paste, including strength, drying shrinkage, creep, and diffusion, it is critical to have a detailed molecular-scale understanding of the behavior of water in nano-confinement and on surfaces of cement paste particles. Structural and dynamic behavior of H_2O molecules and ions at interfaces and in nanopores of a model C-S-H binding phase has been quantified on the basis of molecular dynamics computer simulations using ClayFF [44] and an idealized model of a C-S-H surface based on the tobermorite structure [48,75]. This model assumes a fully polymerized drierkette chain structure. Also in order to have the stoichiometric composition of tobermorite, one half of the non-bridging oxygens of the Si-tetrahedra (those pointing outward from the surface) were assumed to be Si—O—H, while the other half (those pointing parallel to the surface) we assumed to be non-protonated $Si–O^-$ (Fig. 4) Thus, the model surface was considered electrostatically neutral.

The MD simulations were performed in the statistical *NVT* ensemble with a time step of 1 fs, and the equilibrium MD trajectory of the system was recorded for further statistical analysis every 5 fs over a period of 1 ns after a pre-equilibration period of approximately 0.1 ns. The relatively long time scale allows one to accurately quantify the slow diffusional dynamics of H_2O molecules at the tobermorite surface. If the

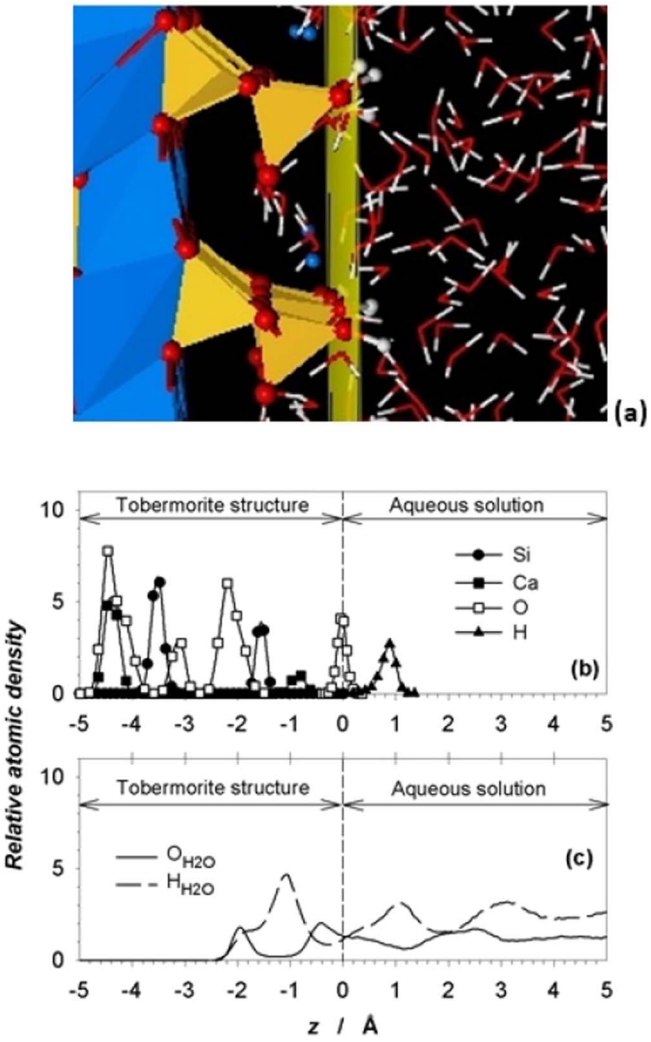

Fig. 4. (a) MD snapshot of H_2O molecules on the surface of tobermorite. The tobermorite substrate is located at negative z values, with Si of the bridging tetrahedra (yellow). The interface ($z = 0$; yellow transparent plane) is nominally defined as the average position of the top-most non-bridging oxygens. (b) Computed atomic density profiles of Si, Ca, O and H atoms at the mineral-water interface. Si of the bridging tetrahedra occurring at −1.6 Å (filled dots). (c) The aqueous layer is generally located at positive z values, but some H_2O molecules can penetrate and remain as deep as −2.5 Å below the nominal interface into the tobermorite structure. (For interpretation of the references to color in this figure legend, the reader is referred to the web version of this article.)

location of the tobermorite-water interface is defined by the average positions of the exterior non-bridging oxygens of the bridging tetrahedra (yellow plane in Fig. 4(a) and dashed vertical lines in Fig. 4(b, c), it is possible to distinguish “external” H_2O molecules, that reside above the interface ($z > 0$) from the “internal” ones that spend most of their time somewhat below the interface ($z < 0$), within channels between the tetrahedral chains on the tobermorite surface. These two types of water molecules are clearly visible in the computed atomic density profiles shown (Fig. 4c) and have very different diffusional behavior. The MD simulations show that the diffusion coefficient for the “external” water molecules is about $D_{ex} = 6 \times 10^{-10}\,m^2\,s^{-1}$, while it is more than an order of magnitude lower for the “internal” H_2O molecules ($D_{in} = 5 \times 10^{-11}\,m^2\,s^{-1}$). Both of these values are much less than the self-diffusion coefficient of bulk liquid water calculated for the same force field ($\sim 3 \times 10^{-9}\,m^2\,s^{-1}$).

The longer-time-scale diffusional dynamics of water at the tobermorite interface can be further quantified by means of the Van Hove self-correlation function (VHSCF) shown in Eq. (11),

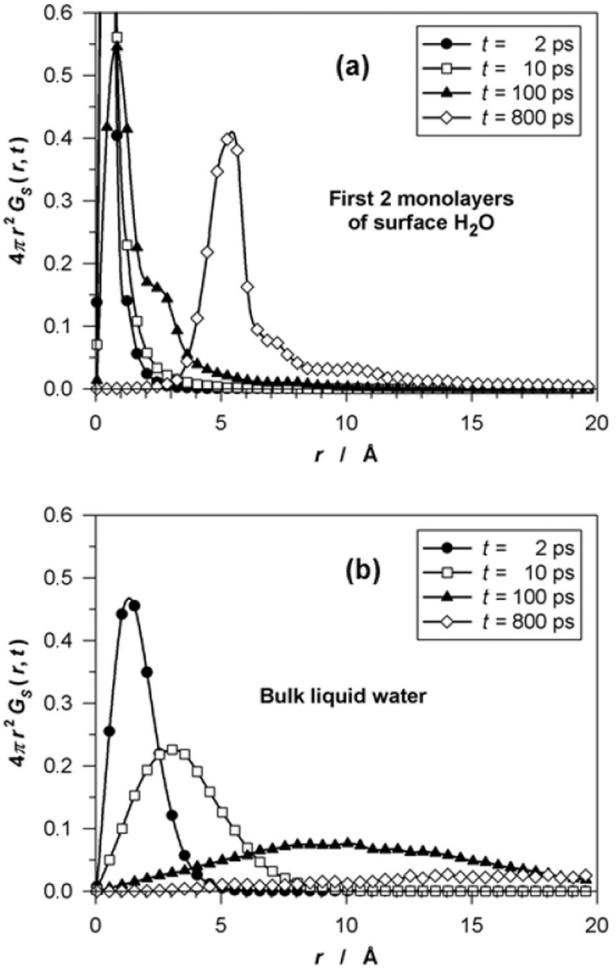

Fig. 5. (a) Van Hove self-correlation functions for the diffusing H_2O molecules in the first two monolayers of water at the surface of tobermorite. The VHSCF corresponding to the isotropic diffusion of H_2O molecules in bulk liquid water is shown in (b) for comparison.

$$G(r,t) = \frac{1}{N}\left\langle \sum_{i=1}^{N} \delta\left[r + r_i(0) - r_i(t)\right] \right\rangle \tag{11}$$

where r is the coordinate of the molecule, t is time, and N is the total number of molecules. This relationship describes the correlation in the positions of the same atom at different times, such that $4\pi r^2 G(r, t)dr$ is the probability of finding an atom at distance r after a time t if the position of this atom was at the origin $r = 0$ at the initial time $t = 0$. The Fourier transform of the VHSCF represents the incoherent or self-intermediate scattering function (SISF), which can be directly measured in incoherent quasielastic neutron scattering experiments and contains detailed information concerning the single-molecule dynamics both in time and space domain. The calculation of this correlation function for the water molecules strongly bound to the surface of tobermorite (within first two monolayers of H_2O at the surface) shows a dramatic difference in the dynamic behavior of adsorbed H_2O, as compared with the diffusional dynamics in bulk liquid water (Fig. 5(a, b)). This yields a characteristic time scale of the diffusional process of the order of $\tau_m \sim 0.8$ ns in excellent agreement with proton field cycling relaxometry NMR measurements, for OPC and other cement phases that indicate a mean residence time of H_2O molecules between diffusional jumps on the surface of ~0.8–1.0 ns [182]. The VHSCF calculation also points to a specific length scale of the H_2O hopping diffusional mechanism ($l_m \sim 5.5$ Å), not unlike the characteristic lattice dimension of crystalline ice between two neighboring strong H-bonding sites (Fig. 5(a) for $t = 800$ ps).

From the 2-dimensional Einstein equation, $D = \langle|r(t) - r(0)|^2\rangle / 4\tau$, the mean time for jumps between surface sites from the NMR results yield a diffusion coefficient of 0.9×10^{-10} m^2 s^{-1}, which is also in remarkable agreement with the average diffusion coefficient for all surface-associated H_2O molecules obtained from MD simulations (1.0×10^{-10} m^2 s^{-1}). Here, r is the mean jump displacement (assumed to be 5.5 Å, from the results of the VHSCF calculations (Fig. 5(a)) and τ is the mean jump time, $\tau \sim \tau_m \sim 0.8$ ns. This level of agreement definitely provides strong support for the molecular scale interpretation of experimental measurements probing the behavior of water in nanoconfinement and on the surfaces of cement paste particles based on MD-simulated data.

5.2. Application of IFF to study cement minerals

5.2.1. Prediction of agglomeration energy of C_3S and C_3A

A major achievement of IFF approach is to provide the most accurate molecular models of cement minerals for computing the surface and interfacial properties [49–51,85,183]. These force field models are also suitable to carry out molecular simulations of inorganic-organic interfaces. For the first time, atomistic models of cement clinkers were simulated to demonstrate that the mode of action of grinding aids used in cement production is to reduce the agglomeration energy between freshly cleaved surfaces [184].

In particular, it could account for the performance of different organic additives as ranked on full scale milling results in cement plants [49,179,185]. A key to this success was a very careful development of force fields of cement minerals using the IFF approach [49–51]. One molecular monolayer of the so-called grinding aids of about 0.5 nm thickness decreases the agglomeration energy by over 95% compared to the original cleavage energy of 1200 and 1300 mJ/m^2 of C_3A and C_3S respectively (Fig. 6). A larger thickness of the organic layer thickness produces no substantial improvement but also no depreciation in grinding performance as noticed in simulation and laboratory studies. The reduction in Coulomb energy is due to the spacer effect of the organic interlayer and minimization of local dipole moments by molecule-specific complexation of surface ions.

5.2.2. Hydration of C_3S in the presence of aluminate ions

Tricalcium silicate is the major constituent of cement clinker, accounting for 50–70% of the mass of Portland cement. It exists in the form of alite in cement as an impure form and serves as a model for Portland cement due to similar reaction kinetics. Despite its practical industrial importance, the kinetics of this reaction are not yet fully understood. Different mechanisms have been proposed based on a kinetic control by diffusion, solubility or crystal nucleation and growth [57,186,187]. We have studied the effect of aluminate ions on the hydration of C_3S. This is an issue of increasing importance in low CO_2 cements where clinker is replaced by supplementary cementitious materials that are often rich in aluminate containing phases. Earlier it was found that a pH sensitive retardation of C_3S hydration by aluminate ions occurs through the formation of Si−O−Al covalent at the outermost surface of C_3S, but that the amount of the hydrates formed increases at a later stage [57,188].

Our molecular dynamics simulations help to establish that aluminates can adsorb on hydroxylated C_3S mainly through strong ionic interactions between aluminate and calcium ions, as well as to the formation of hydrogen bonds with silicate surface groups (Al−OH⋯O$^-$−Si and Al−OH⋯OH−Si) at the interface below pH 13 [85]. Aluminate ions were observed in direct contact (at distance ≤ 3 Å) with the hydroxylated C_3S surface along with a strongly negative adsorption energy of −24 kcal/mol (Fig. 7a). Presence of more dissolved Ca^{2+} and OH^- and surface reorganization reduce the adsorption energy to only −6 kcal/mol (Fig. 7b). It could therefore be inferred that it is these adsorbed complexes that inhibit C_3S hydration, blocking reactive areas and/or sites in a similar way as recently

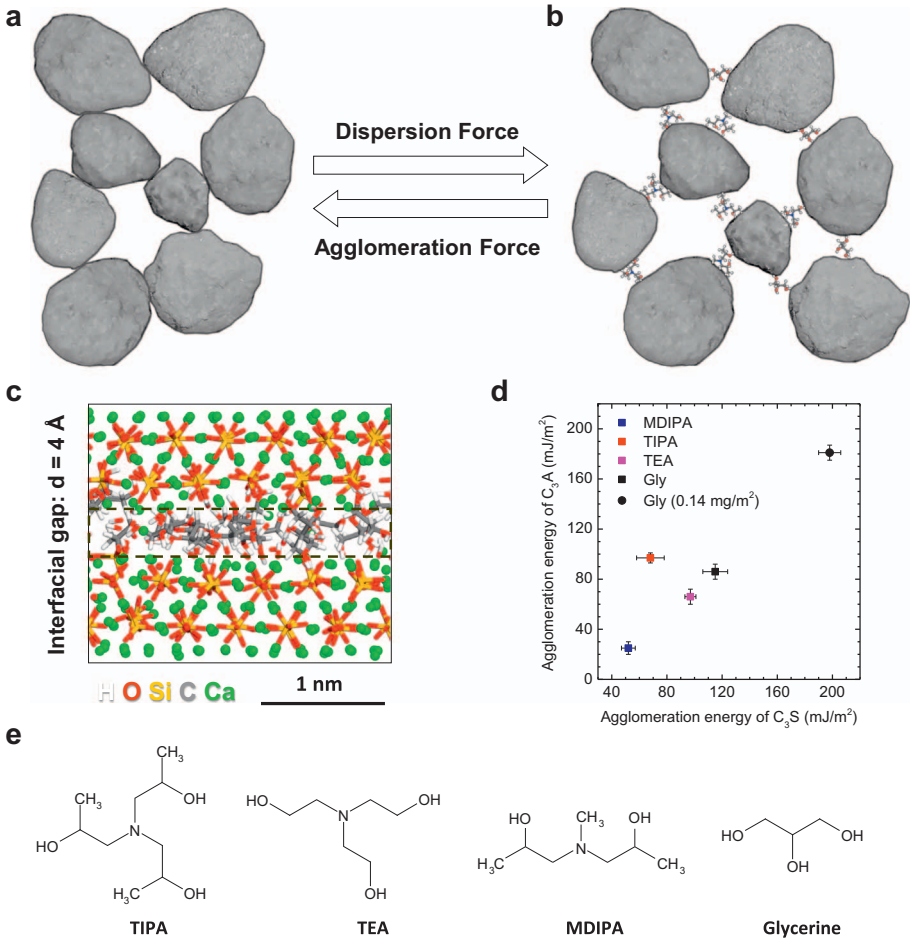

Fig. 6. Modification of clinker particle agglomeration forces by organic additives (grinding aids) during comminution in industrial cement mills using molecular dynamics simulations. (a) Schematic diagram of agglomeration of clinker particles. (b) A conceptual image is presented to show the dispersion of clinker particles in the presence of grinding aids (organic additives). (c) Two tricalcium silicate (C_3S) surfaces with an intermediate monolayer of glycerine molecules. The presence of organic molecules creates an interfacial gap between tricalcium silicate surfaces that lowers agglomeration energies up to 90% in comparison to the neat mineral surfaces. (d) Computed agglomeration energy due to presence of commercial GAs with chemical dosage of 20 mg/m^2 for C_3A and C_3S. (e) Structure of common chemical additives to reduce the energy required for grinding of cement, including triisopropanolamine (TIPA), triethanolamine (TEA), *N*-methyl-diisopropanolamine (MDIPA), and glycerine.
(Adapted from [refs. 49, 50, 185]).

proposed for polycarboxylate comb-copolymers [20]. Importantly, the same MD simulations show that above pH 13, calcium aluminate complexes form in solution but not at the C_3S surface (Fig. 7d), which offers a fully consistent picture of retardation by aluminates and its pH dependence. Our results provide fundamental understanding on how ions in solutions can affect the dissolution of silicates in alkaline media, a result of interest to various fields beyond cement science such as geochemistry and environmental sciences.

5.3. Adsorption of ions and stable complexes on portlandite surfaces using CementFF

The force field has been used to study the atomistic mechanisms of the growth of portlandite under different conditions using metadynamics calculations. Experimentally observed changes in portlandite morphology with changing pH reported in literature have been linked to different growth mechanisms at different surfaces being controlled by either Ca^{2+} or OH^- [46,106]. In the presence of silica, a stable calcium silicate complex has been identified, which can play a critical role in the initial growth of portlandite and C-S-H (Fig. 8) [154]. This calcium silicate complex was found to adsorb on surfaces of portlandite, giving insights into the growth of portlandite in cement hydration. Based on computed free energies of adsorption and approximate residence time, it was possible to propose an atomistic mechanism of poisoning of portlandite growth by the adsorption of the calcium silicate complex, an effect which is also experimentally observed [154,189–191].

Recently, Kumar et al. have synthesized compositionally uniform high Ca/Si ratio synthetic C-S-H phases without invoking a secondary portlandite phase [192]. The proposed atomistic structures of C-S-H with Ca/Si ratios ranging from 1.25 to 2.0 with constraints derived from ^{29}Si DNP NMR (dynamic nuclear polarization) and DFT were tested with classical MD simulations using CementFF. These structures were found to be stable with realistic bond lengths and coordination geometries. Additionally, the potential function is currently being used to study single defects in a tobermorite bulk cell. The stability of these single defects has been calculated and compared with DFT showing good agreement structurally and energetically.

5.4. Application of ReaxFF to study calcium silicates hydration

The main advantage of ReaxFF over other force fields relies on its capacity to reproduce chemical reactions and transition states with comparable accuracy to DFT methods, yet several orders of magnitude faster. In cement, chemical reactions are ubiquitous during service life of the material, but possibly the most important stage is early cement hydration. Despite the vast number of investigations on the topic, the fundamental aspects of the hydration kinetics are still under debate [10,13,193–195].

The use of molecular simulation to investigate cement hydration has started quite recently. Several researchers used DFT methods to simulate bulk tricalcium silicate [32,196–198], dicalcium silicate [32,199], and tricalcium aluminate [200], seeking a relationship between their reactivity and bulk electronic properties, moving from bulk crystals to surfaces, and also cleavage energies of C_3S [156] and β-γ-C_2S polymorphs [201] to determine the stability of the surfaces, and estimate their relative reactivity. The detailed mechanism of water adsorption on C_2S surfaces and the reaction energy barriers of a single water molecule dissociation have also been computed [201]. The high computational cost of DFT simulations makes difficult to go beyond these studies, and

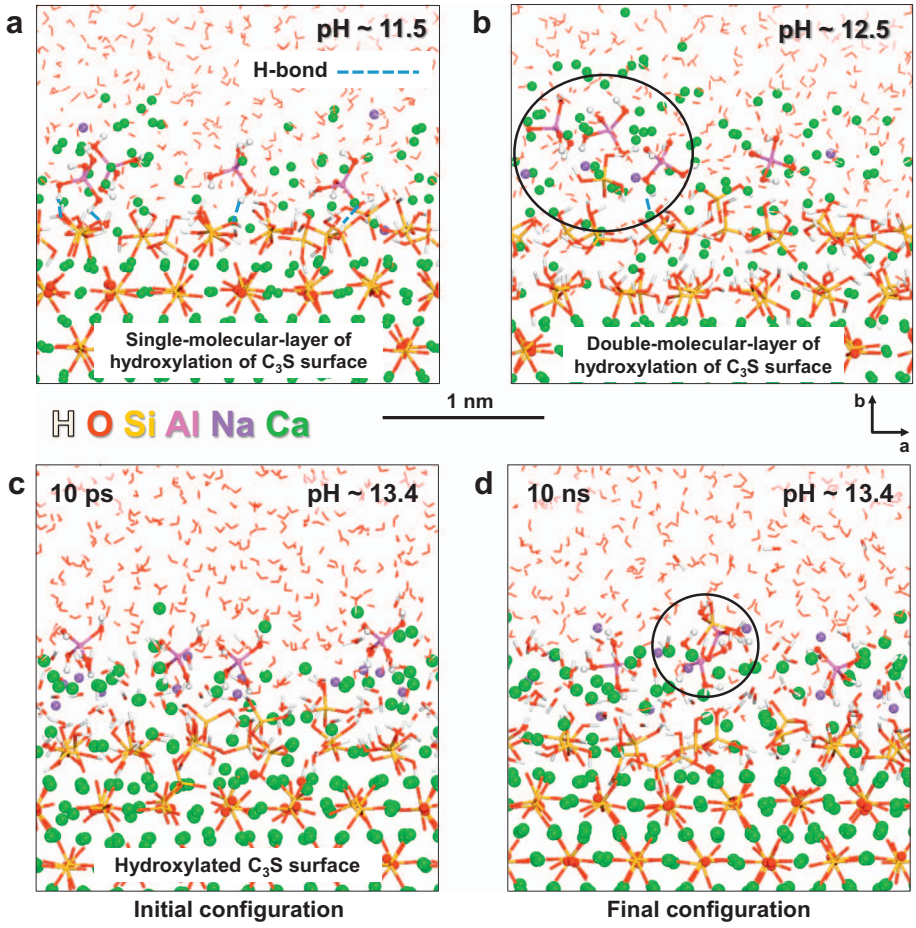

Fig. 7. Interactions of aluminate ions with the hydroxylated C_3S surface according to molecular dynamics simulation. (a) Interactions of aluminate ions with the initially hydrated C_3S surface (one molecular layer) at pH ~ 11.5 involve strong bonding to calcium ions on the surface as well as interfacial hydrogen bonds (Al—OH···O^-—Si and Al—OH···OH—Si). (b) Interactions of aluminate ions with the C_3S surface after double-layer hydration at pH ~12.5 are weaker. Dissolution of silicate ions and formation of ionic complexes between aluminate and calcium ions, aluminate ions and silicate ions (circular highlight), (c) Aluminate ions on the hyd. C_3S surface with added NaOH at pH 13.4 as seen. Initial position of aluminate ions and NaOH on the hyd. C_3S ($SiO(OH)_3^{1-}$) surface (after 10 ps). (d) Equilibrium positions of aluminate ions and NaOH on the hyd. C_3S ($SiO(OH)_3^{1-}$) surface (after 10 ns). Surface reconstruction and complex formation between aluminate and silicate ions can be seen (circular highlight). NaOH weakens the interactions between aluminate ions with Ca^{2+} and silicate ions of the hydrated C_3S surface, shifting the equilibrium towards aluminate desorption [ref 85].

makes it necessary to use empirical force fields to account for the large number of atoms and surface relaxation times involved during cement hydration.

ReaxFF can overcome this limitation. A good example is the topochemical vapor phase hydration of lime. Calcium oxide has a very favorable cleavage through the (001) surface, which readily reacts with water vapor even at very low relative humidity [202]. We used ReaxFF to investigate CaO vapor phase hydration at room temperature and pressure in the (001) surface by molecular dynamics [45]. We placed 16 water molecules/nm^2 in contact with the surface and followed the reactions during 2 ns (Fig. 9). The first reactions are extremely fast as all possible reactive sites are free, and slow down as the coverage

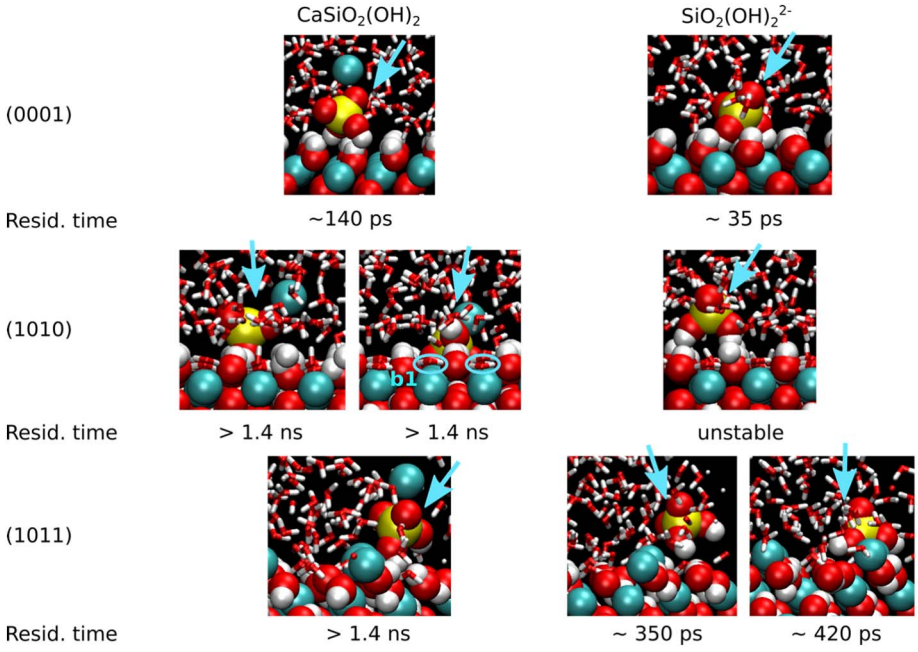

Fig. 8. Adsorption sites for $CaSiO_2(OH)_2$ and $SiO_2(OH)_2^{2-}$ ions at different portlandite surfaces identified by metadynamics calculations. Approximate residence time of each species on that specific surface from MD simulations is also indicated. At (0001) surface both the species are found to have some mobility while residence time of > 1.4 ns indicates a stable and strongly adsorbed site. b1 is the strongly bound water site. Yellow: Si, red: O, white: H, turquoise: Ca. Adapted from [ref 154]. (For interpretation of the references to color in this figure legend, the reader is referred to the web version of this article.)

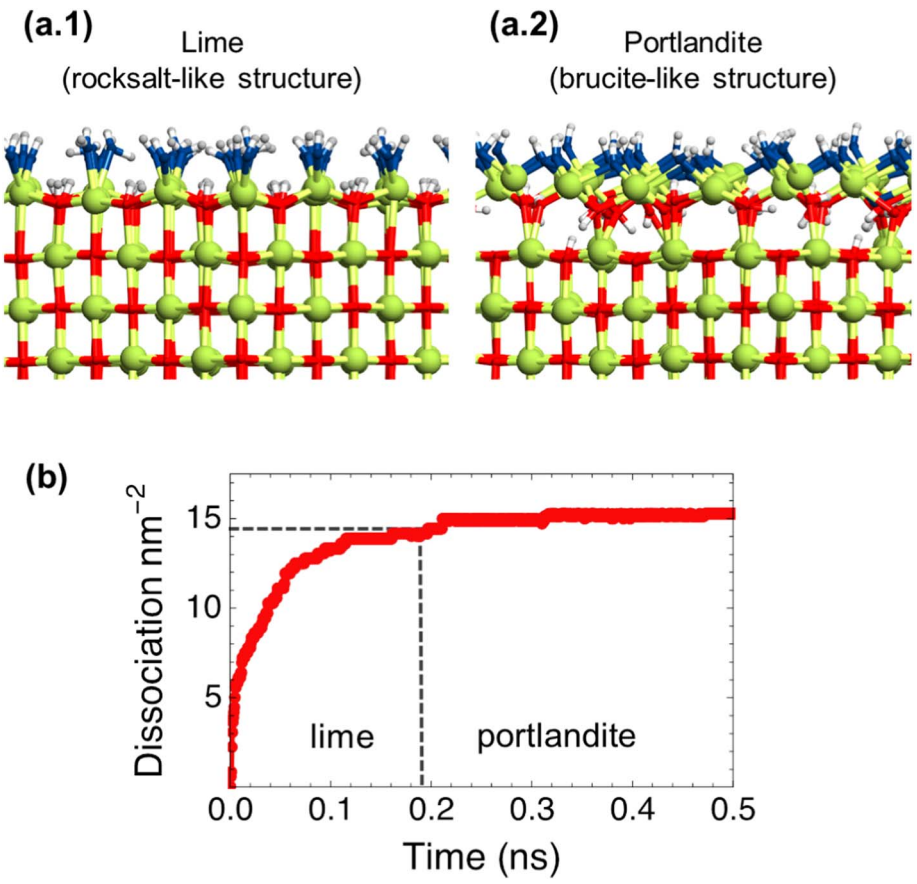

Fig. 9. (a) Snapshots of the simulation. Ca is represented as green spheres, H as white spheres, and oxygen atoms from the solid and from water as red and blue spheres respectively. (a.1) Shows the structure at 0.15 ns, when water has reacted with the surface but the lime structure is maintained. (a.2) shows the structure at 0.25 ns, when the top layer has transform into portlandite. (b) Amount of water dissociated per nm^2 as a function of time. (For interpretation of the references to color in this figure legend, the reader is referred to the web version of this article.)

increases. The most interesting effect takes place when ~14 water molecules/nm^2 have reacted, at 0.19 ns, when the upped crystal layer undergoes a topological change in which the cubic rock salt-like CaO structure evolves towards the hexagonal brucite-like $Ca(OH)_2$ structure. Predicting such an interplay between chemical reactions and structural change is not intuitive, but ReaxFF allows the observation and quantification of physical process without the need of an initial guess. Indeed, there is much experimental evidence indicating that the hydration mechanism of CaO in presence of water vapor is a solid state reaction from CaO to $Ca(OH)_2$ as predicted by the simulations [203–205].

Similar studies were carried out to understand the difference in reactivity between β- and γ-C_2S polymorphs [58,201]. Fig. 10(a) shows a projection of the water adsorption energies over β-C_2S (010) and γ-C_2S (001) surfaces. ReaxFF simulations predict more favorable water adsorption on the less reactive phase, γ-C_2S. This reaction was found spontaneous, i.e. without an energy barrier, at some spots of the γ-C_2S surface, while none of them were found in β-C_2S. However, when water molecules were allowed to react with the surface at room temperature and pressure, we observe an interesting phenomenon. The very first water dissociation reactions were faster in γ-C_2S, but soon after them the reaction rate slows down and a steady state is reached when the favorable spots are saturated. In β-C_2S the initial reactions took place slightly slower, but more reactions take place before the rate slows down, and the saturation is reached when twice as many water molecules react. This suggests that the number of reactive points could be a key feature controlling dissolution. Due to the lower number of reactive points and its fast saturation it would be more difficult to destabilize the γ-C_2S crystal and start desorbing its constituent ions.

Dissolution studies have also been carried out for C_3S. In this case, four different surfaces were investigated in contact with bulk water. To analyze the hydration mechanism, the time-resolved atomic density profiles were computed, i.e. the number of atoms in a volume slice at certain distance from the surface as a function of time (Fig. 11). First, the water molecules dissociate to form surface hydroxyl groups. Then, the hydrogen atoms hop towards inner oxygen atoms, a process equivalent to proton diffusion in bulk oxides [206,207], and leave the surface oxygen atoms free for a subsequent water dissociation reaction. As hydrogen diffuses into the solid, the silicate groups are saturated with protons, screening the SiO-Ca interaction, and Ca atoms start to diffuse towards the solution. Such a mechanism has been previously proposed for oxide minerals and clusters, and it is known as proton-metal exchange [208] and can be simply understood as a replacement of a Ca^{2+} cations by $2H^+$. It is interesting to note that during the very first dissolution, Ca atoms diffuse from the surface but SiO_4^{4-} groups do not, probably due to their size and lower solvation energy in water. As a consequence of the faster leaching of Ca, the C_3S forms a half a nanometer thick *Si*-rich layer in the surface.

5.5. Applications and transferability of C-S-H FF potential

C-S-H FF potential has been widely used in the community because of its good representation of cementitious material benchmarks while presenting a simple formulation and implementation. Using C-S-H FF, various properties are simulated in both the Portland cement family and hybrid cement-based materials. Below is a brief summary of recent applications of C-S-H FF:

(1) The effect of confined water in various C-S-H structures [35,57,130,209–212], which led to discovering the crucial role the water played in C-S-H.
(2) Mechanical properties of various hydrated calcium-silicate materials including > 100 combinatorial defective C-S-H models with various stoichiometries and hydration degrees [125,213], the

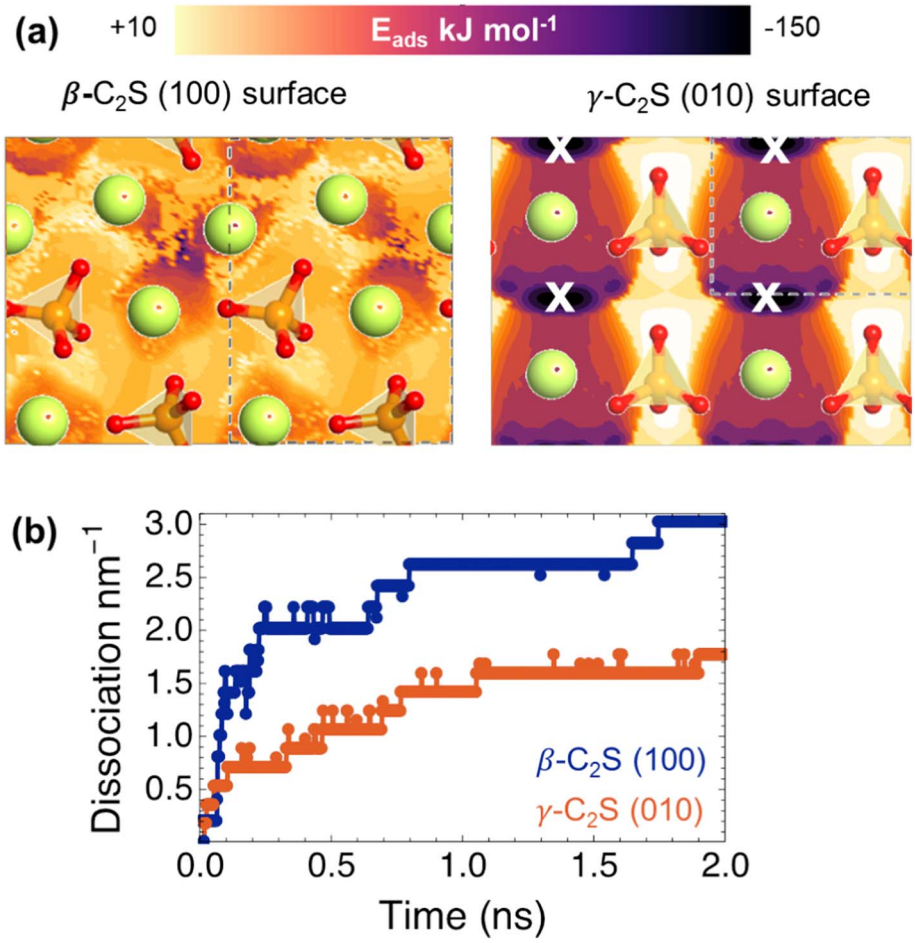

Fig. 10. (a) Adsorption energy map projected over the studied β-C_2S and γ-C_2S surfaces. The Ca^{+2} atoms are represented as green spheres and the SiO_4^{-4} groups as orange tetrahedra with the oxygen atom in red and the silicon in orange. The color scale indicates the water adsorption energy at every specific point of the surface. In γ-C_2S, the crosses show spots where the water molecule reacts spontaneously, i.e. without energy barrier. (b) Number of water dissociation reactions per surface area as a function of time in β-C_2S and γ-C_2S surfaces. (For interpretation of the references to color in this figure legend, the reader is referred to the web version of this article.)

mechanical deformations under tension/compression/shear [214], drying shrinkage [34], friction and scratch behaviors [215], fracture properties [214,216], nano-indentation properties [217] and motions of screw dislocations (Fig. 12) [218].

(3) Thermal expansion and specific-heat capacities of calcium silicate hydrates, showing a good agreement between the simulation results and available experimental measurements [219].

This consistency with experimental data indicates that the strategy of incorporating higher-order properties such as elastic constant in parameterization of CSH-FF improves its predictive capability with regards to phonon vibrations as well.

(4) CSH-FF was not only used in C-S-H phases as mentioned above, but it's also employed in various other cases such as portlandite [220], alite/belite [219], and tobermorite [43,219], or in hybrid cementitious materials where the C-S-H were interacting with nanomaterials such as hexagonal boron nitride [221], graphene/graphene oxide [222], polymers [223], carbon nanotube [224] and other systems [66].

In summary, CSH-FF is a simple yet accurate and computationally very efficient potential customized for cement-based materials to predict various properties such as structural, mechanical, thermal and other properties. Its strength lies in (a) its accurate parameterization which incorporates both structural data and higher order properties such as 21 elastic constants obtained from ab-initio calculations, (b) its computational efficiency, which is ~10 times faster than ReaxFF potential [45,62] for cement and ~2–3 times faster than core-shell potentials [61], and (c) its simple formulation, which is akin to the ClayFF potential. This makes it very easy to implement in various codes and its integration with other force fields to simulate hybrid materials. With such advantages, CSH-FF is a very popular simulation engine in the cement community.

6. Conclusions

This article has been based on information provided at cemff database (http://cemff.epfl.ch) with inputs from all contributing authors. This article is the first available to date which discusses the many different force field parameterized potentials and their validations for important classes of cementitious materials. This online force field database can be used to provide guidelines for future research. It can be also expanded to include more refined models of cementitious materials for applications in the field of geochemistry, environmental sciences, cement–waste interactions and other structural materials. The ***cemff*** database can help users to choose the best possible option to model their system of interest.

From the different force field types mentioned in this article, the following major conclusions can be drawn:

1. Generally speaking, each force field parameterization is most reliable for the properties and phenomena they have been validated to reproduce the experimental data. There is no single force field that is best for all applications and phenomena. As an example, CSH-FF is fitted to several ab-initio-based lattice parameters and elastic constants of tobermorite, thus it does an excellent job in predicating equilibrium and mechanical properties of C-S-H phases. However, it cannot predict reactive phenomena. On the other hand, reactive potentials such as ReaxFF is parameterized to several ab-initio

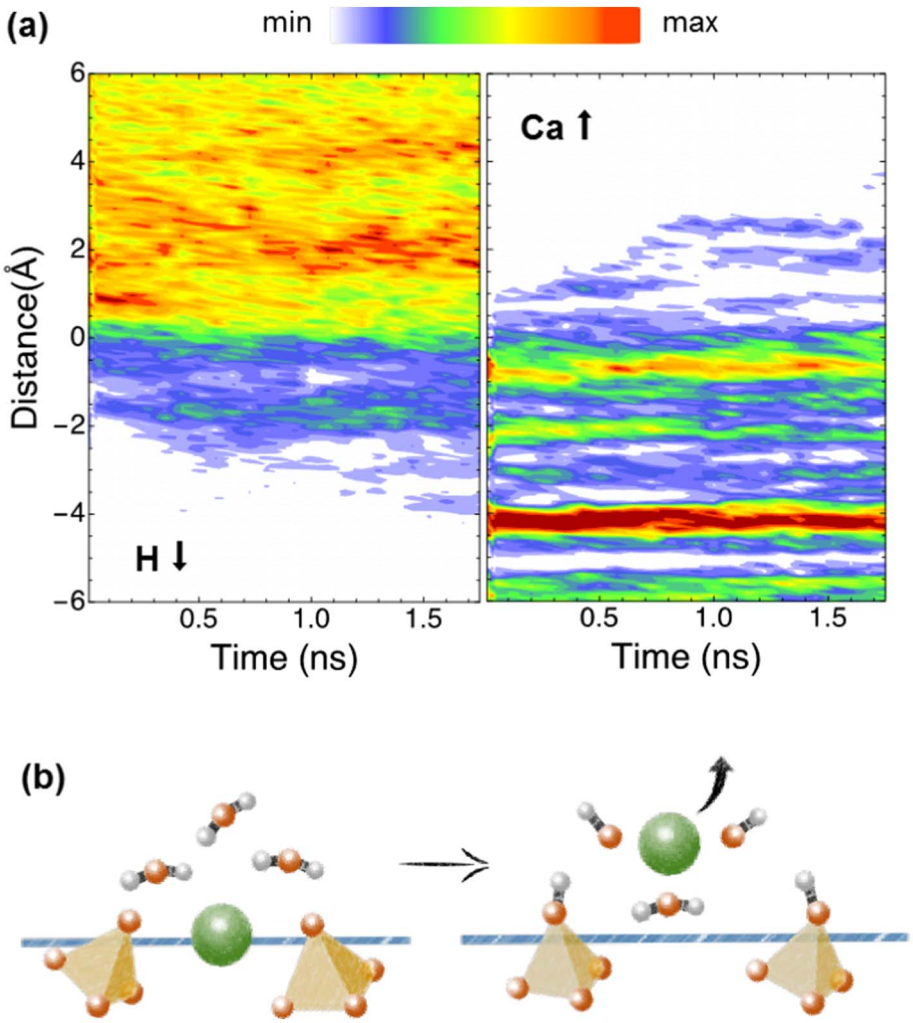

Fig. 11. (a) Time resolved atomic density profiles of H and Ca on C_3S (010) surface. The distance origin shows the position of the Gibbs plane defining the position of the surface before hydration. Hence, negative values indicate positions inside the crystals. The color scale represents the element-normalized number of atoms at a given distance from the surface. (b) Schematic representation of the hydration process.

simulations based on bond-formation/breakages, hence it is quite useful for reactive mechanisms while the mechanical properties may not be accurate. Therefore, for a complex system that involves prediction of both chemical reactions and mechanical properties, a use of a hybrid strategy is recommend [125].

2. ClayFF accurately describes the bulk structures of a broad range of simple hydroxide and oxyhydroxides phases. Parametrization of ClayFF using a set of simple structurally well-characterized hydrated phases allows good transferability of the force field parameters.
3. IFF provides the physically and chemically most consistent parameters. It quantitatively describes chemical bonding via reliable partial atomic charges, and enables accurate simulations of both bulk properties and interfacial properties of cement minerals in the presence of different mineral phases, water, and polymers. The thermodynamically consistent IFF parameters reproduce a wide range of properties such as dipole moments, lattice constants, density, cleavage energy, solid – water interface tensions, hydration energy (for stable, nonreactive surfaces), anisotropies of interfacial energies for individual crystal facets, structural properties (IR and Raman spectra), thermal and elastic constants in excellent agreement with experimental measurements. IFF can be extended to simulate reactions and explore reaction mechanisms as chemical bonding in the continuous spectrum from covalent bonding to ionic bonding is well described. IFF routinely includes validations of surface and interfacial properties, and accurately reproduces cleavage energies, hydration energies, and contact angles.
4. The CementFF is simple and hence flexible force field that represents well many different minerals of interest in calcium silicate systems and allows a first approach to interfacial properties at low computational cost. A single description of elemental species within a water-solid system gives a good insight into the possible mechanisms at the atomic level [154]. The major limitation is that since the atoms within a system (except for oxygen atoms of the hydroxyl and water) are not heavily constrained through different partial atomic charges and their corresponding interactions fitted to that system, the simulation results are expected to have some degree of deviation (< 10%).
5. ReaxFF is able to reproduce with good accuracy the energy of the first solvation shell, chemical reactions associated with pH change (proton transfer), structural and elastic properties. It allows the computation of surface energies of inorganic compounds and also helps in understanding the surface reactivity of the material.
6. ClayFF and CSH-FF parameters for cementitious minerals have not been well validated for surface and interfacial properties. Without extensive validations of surface and interfacial properties of minerals, it is difficult to predict reliable data on adsorption energy of inorganic and organic molecules on the mineral surface in agreement with experiment.
7. ClayFF is an easily implemented and computationally low-cost force field which probably needs some reparametrization to make it suitable for further more ambitious applications. For example, in the case of tobermorite minerals, C-S-H FF model improved the atomic charges and non-bonded (LJ) interaction parameters of

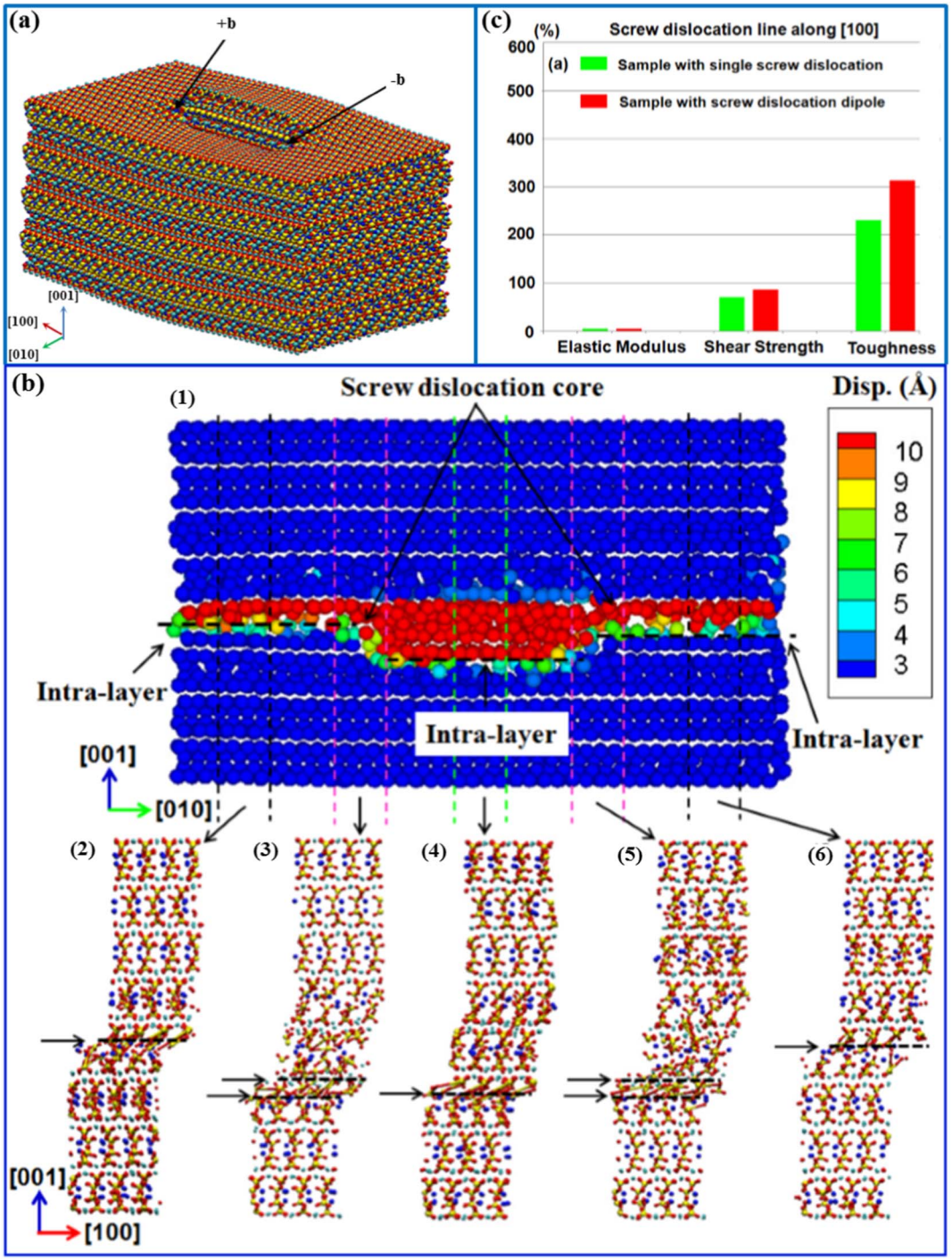

Fig. 12. (a) Atomic configurations of the super cell of tobermorite samples containing screw dislocation dipole with opposite signs, + b and –b. The dislocation line is along [001]. (b) Atomic configurations of tobermorite with screw dislocation dipole along [100] at strain of 10.0%. The atoms in (1) are colored by their displacement deviation. (2–6) shows the cross-sectional atomic views along [010] at various locations. The dash lines and arrows in (2–6) denote the gliding planes. (c) Comparisons of the effects of single screw dislocation and dislocation dipole on elastic modulus, shear strength and toughness. The vertical axis stands for the percentage of increased mechanical properties with respect to those measured from the defect-free tobermorite. Adapted from [ref 218]. (For interpretation of the references to color in this figure legend, the reader is referred to the web version of this article.)

species used in the ClayFF model.

8. One principal limitation of non-reactive classical force fields such as ClayFF, IFF, CementFF, and CSH-FF is that they do not simulate chemical reactions which involve the formation or dissociation of chemical bonds. The ReaxFF force field overcomes this limitation and simulates chemical reaction successfully. But it has limitations with atomic charge calculations and predicting mechanical properties, as it does not incorporate the polarizable charge transfer model or use mechanical properties as observables for fitting.
9. Specialized energy expressions of intermolecular potentials (Buckingham as well as ReaxFF) are typically limited in compatibility with other harmonic energy expressions (PCFF, CHARMM, AMBER, COMPASS, GROMACS, and OPLS-AA). In this scenario it is difficult to use these interatomic potential parameters to study the interactions between biomolecules and cementitious minerals.
10. ClayFF and CSH-FF neglect the nature of chemical bonding which is predominantly covalent and only partially ionic for most silicates present in the inorganic minerals. Even Born–Mayer–Huggins,

GULP, and Buckingham potentials do not adequately consider the balance of covalent and ionic contributions to chemical bonding present in the mineral.

11. In the case of IFF models, remaining uncertainties in atomic charges are 5–10%, at most ± 0.1e, which are much smaller than with other methods (DFT-derived up to ± 1.0e). Lennard-Jones parameters for the mineral remain adjustable in a certain range with similar performance. Transferability of the parameters to other harmonic energy expressions may lead up to 10% differences in the values of mechanical and thermal properties.

The authors hope that this general overview and with the use of the ***cemff*** database, improved and more accurate force fields can be developed. This may be used in many specific applications in cementitious systems and also be of use to wider audiences interested in mineral interfaces.

Acknowledgements

R.K.M. and R.J.F. acknowledge research support from Commission for Technology Innovation (CTI project number 15846.1) and Swiss Competence Center for Energy Research – Supply of Electricity (SCCER-SoE) is also acknowledged. H.M. acknowledges the financial support from the Departamento de Educación, Política Lingüística y Cultura del Gobierno Vasco (IT912-16) and the ELKARTEK program. R.S. acknowledges support from National Science Foundation (NSF) Grant Nos. CMMI-1235522 and CMMI-1538312. A.K.M. acknowledges financial support from Swiss National Foundation (Grant No. 153044). S.G. would like to thank the industrial-academic research network Nanocem for funding. T.J. and H.H. acknowledge support by the ACS Petroleum research fund ACS-PRF (54135-ND10) and the National Science Foundation (DMREF 1623947 and CBET 1530790). A.G.K. acknowledges support by the industrial chair “Storage and Disposal of Radioactive Waste” at the Institut Mines-Télécom Atlantique, funded by ANDRA, Areva, and EDF.

Appendix A. Supplementary data

Supplementary data to this article can be found online at https://doi.org/10.1016/j.cemconres.2017.09.003.

References

[1] K. Scrivener, The concrete conundrum, Chem. World 5 (2008) 62–66.
[2] E. Gartner, H. Hirao, A review of alternative approaches to the reduction of CO_2 emissions associated with the manufacture of the binder phase in concrete, Cem. Concr. Res. 78 (2015) 126–142.
[3] R.J. Flatt, N. Roussel, C.R. Cheeseman, Concrete: an eco material that needs to be improved, J. Eur. Ceram. Soc. 32 (2012) 2787–2798.
[4] B. Lothenbach, K. Scrivener, R.D. Hooton, Supplementary cementitious materials, Cem. Concr. Res. 41 (2011) 1244–1256.
[5] R. Snellings, G. Mertens, J. Elsen, Supplementary cementitious materials, Rev. Mineral. Geochem. 74 (2012) 211–278.
[6] R. Khatri, V. Sirivivatnanon, W. Gross, Effect of different supplementary cementitious materials on mechanical properties of high performance concrete, Cem. Concr. Res. 25 (1995) 209–220.
[7] H. Toutanji, N. Delatte, S. Aggoun, R. Duval, A. Danson, Effect of supplementary cementitious materials on the compressive strength and durability of short-term cured concrete, Cem. Concr. Res. 34 (2004) 311–319.
[8] M.A. Megat Johari, J.J. Brooks, S. Kabir, P. Rivard, Influence of supplementary cementitious materials on engineering properties of high strength concrete, Constr. Build. Mater. 25 (2011) 2639–2648.
[9] H.F. Taylor, Cement Chemistry, Thomas Telford, 1997.
[10] P. Juilland, E. Gallucci, R. Flatt, K. Scrivener, Dissolution theory applied to the induction period in alite hydration, Cem. Concr. Res. 40 (2010) 831–844.
[11] A.J. Allen, J.J. Thomas, H.M. Jennings, Composition and density of nanoscale calcium-silicate-hydrate in cement, Nat. Mater. 6 (2007) 311–316.
[12] E. Pustovgar, R.P. Sangodkar, A.S. Andreev, M. Palacios, B.F. Chmelka, R.J. Flatt, J.-B. d'/Espinose de Lacaillerie, Understanding silicate hydration from quantitative analyses of hydrating tricalcium silicates, Nat. Commun. 7 (2016).
[13] J.W. Bullard, H.M. Jennings, R.A. Livingston, A. Nonat, G.W. Scherer, J.S. Schweitzer, K.L. Scrivener, J.J. Thomas, Mechanisms of cement hydration, Cem. Concr. Res. 41 (2011) 1208–1223.
[14] X. Cong, R.J. Kirkpatrick, 29 Si MAS NMR study of the structure of calcium silicate hydrate, Adv. Cem. Based Mater. 3 (1996) 144–156.
[15] B. Lothenbach, T. Matschei, G. Möschner, F.P. Glasser, Thermodynamic modelling of the effect of temperature on the hydration and porosity of Portland cement, Cem. Concr. Res. 38 (2008) 1–18.
[16] B. Lothenbach, A. Nonat, Calcium silicate hydrates: solid and liquid phase composition, Cem. Concr. Res. 78 (Part A) (2015) 57–70.
[17] K. Yamada, T. Takahashi, S. Hanehara, M. Matsuhisa, Effects of the chemical structure on the properties of polycarboxylate-type superplasticizer, Cem. Concr. Res. 30 (2000) 197–207.
[18] R.J. Flatt, I. Schober, E. Raphael, C. Plassard, E. Lesniewska, Conformation of adsorbed comb copolymer dispersants, Langmuir 25 (2009) 845–855.
[19] R.K. Mishra, D. Geissbuhler, H.A. Carmona, F.K. Wittel, M.L. Sawley, M. Weibel, E. Gallucci, H.J. Herrmann, H. Heinz, R.J. Flatt, En route to multi-model scheme for clinker comminution with chemical grinding aids, Adv. Appl. Ceram. 114 (2015) 393–401.
[20] D. Marchon, P. Juilland, E. Gallucci, L. Frunz, R.J. Flatt, Molecular and submolecular scale effects of comb-copolymers on tri-calcium silicate reactivity: toward molecular design, J. Am. Ceram. Soc. 100 (2017) 817–841.
[21] I.G. Richardson, Tobermorite/jennite- and tobermorite/calcium hydroxide-based models for the structure of C-S-H: applicability to hardened pastes of tricalcium silicate, β-dicalcium silicate, Portland cement, and blends of Portland cement with blast-furnace slag, metakaolin, or silica fume, Cem. Concr. Res. 34 (2004) 1733–1777.
[22] U. Angst, B. Elsener, C.K. Larsen, Ø. Vennesland, Critical chloride content in reinforced concrete — a review, Cem. Concr. Res. 39 (2009) 1122–1138.
[23] C.D. Lawrence, Sulphate attack on concrete, Mag. Concr. Res. 42 (1990) 249–264.
[24] A. Neville, The confused world of sulfate attack on concrete, Cem. Concr. Res. 34 (2004) 1275–1296.
[25] M.L.D. Gougar, B.E. Scheetz, D.M. Roy, Ettringite and C·S·H Portland cement phases for waste ion immobilization: a review, Waste Manag. 16 (1996) 295–303.
[26] I. Androniuk, C. Landesman, P. Henocq, A.G. Kalinichev, Adsorption of gluconate and uranyl on C-S-H phases: combination of wet chemistry experiments and molecular dynamics simulations for the binary systems, Phys. Chem. Earth A/B/C 99 (2017) 194–203.
[27] E. Wieland, J. Tits, M.H. Bradbury, The potential effect of cementitious colloids on radionuclide mobilisation in a repository for radioactive waste, Appl. Geochem. 19 (2004) 119–135.
[28] N.D.M. Evans, Binding mechanisms of radionuclides to cement, Cem. Concr. Res. 38 (2008) 543–553.
[29] E. Nadgornyi, Dislocation dynamics and mechanical properties of crystals, Prog. Mater. Sci. 31 (1988) 1–530.
[30] E.B. Tadmor, R. Phillips, M. Ortiz, Mixed atomistic and continuum models of deformation in solids, Langmuir 12 (1996) 4529–4534.
[31] N. Burlion, F. Skoczylas, T. Dubois, Induced anisotropic permeability due to drying of concrete, Cem. Concr. Res. 33 (2003) 679–687.
[32] H. Manzano, E. Durgun, M.J. Abdolhosseine Qomi, F.-J. Ulm, R.J.M. Pellenq, J.C. Grossman, Impact of chemical impurities on the crystalline cement clinker phases determined by atomistic simulations, Cryst. Growth Des. 11 (2011) 2964–2972.
[33] H. Manzano, E. Masoero, I. Lopez-Arbeloa, H.M. Jennings, Shear deformations in calcium silicate hydrates, Soft Matter 9 (2013) 7333–7341.
[34] M.B. Pinson, E. Masoero, P.A. Bonnaud, H. Manzano, Q. Ji, S. Yip, J.J. Thomas, M.Z. Bazant, K.J. Van Vliet, H.M. Jennings, Hysteresis from multiscale porosity: modeling water sorption and shrinkage in cement paste, Phys. Rev. Appl. 3 (2015) 064009.
[35] D. Hou, H. Ma, Y. Zhu, Z. Li, Calcium silicate hydrate from dry to saturated state: structure, dynamics and mechanical properties, Acta Mater. 67 (2014) 81–94.
[36] S. Bishnoi, K.L. Scrivener, Studying nucleation and growth kinetics of alite hydration using μic, Cem. Concr. Res. 39 (2009) 849–860.
[37] J.J. Thomas, J.J. Biernacki, J.W. Bullard, S. Bishnoi, J.S. Dolado, G.W. Scherer, A. Luttge, Modeling and simulation of cement hydration kinetics and microstructure development, Cem. Concr. Res. 41 (2011) 1257–1278.
[38] J.W. Bullard, G.W. Scherer, J.J. Thomas, Time dependent driving forces and the kinetics of tricalcium silicate hydration, Cem. Concr. Res. 74 (2015) 26–34.
[39] K. Ioannidou, K.J. Krakowiak, M. Bauchy, C.G. Hoover, E. Masoero, S. Yip, F.-J. Ulm, P. Levitz, R.J.-M. Pellenq, E. Del Gado, Mesoscale texture of cement hydrates, Proc. Natl. Acad. Sci. 113 (2016) 2029–2034.
[40] L. Liu, A. Jaramillo-Botero, W.A. Goddard, H. Sun, Development of a ReaxFF reactive force field for ettringite and study of its mechanical failure modes from reactive dynamics simulations, J. Phys. Chem. A 116 (2012) 3918–3925.
[41] S. Piana, J.D. Gale, Three-dimensional kinetic Monte Carlo simulation of crystal growth from solution, J. Cryst. Growth 294 (2006) 46–52.
[42] P. Raiteri, R. Demichelis, J.D. Gale, Thermodynamically consistent force field for molecular dynamics simulations of alkaline-earth carbonates and their aqueous speciation, J. Phys. Chem. C 119 (2015) 24447–24458.
[43] R. Shahsavari, R.J.M. Pellenq, F.-J. Ulm, Empirical force fields for complex hydrated calcio-silicate layered materials, Phys. Chem. Chem. Phys. 13 (2011) 1002–1011.
[44] R.T. Cygan, J.-J. Liang, A.G. Kalinichev, Molecular models of hydroxide, oxyhydroxide, and clay Phases and the development of a general force field, J. Phys. Chem. B 108 (2004) 1255–1266.
[45] H. Manzano, R.J.M. Pellenq, F.-J. Ulm, M.J. Buehler, A.C.T. van Duin, Hydration of calcium oxide surface predicted by reactive force field molecular dynamics, Langmuir 28 (2012) 4187–4197.

[46] S. Galmarini, A. Aimable, N. Ruffray, P. Bowen, Changes in portlandite morphology with solvent composition: atomistic simulations and experiment, Cem. Concr. Res. 41 (2011) 1330–1338.
[47] H. Heinz, H. Ramezani-Dakhel, Simulations of inorganic-bioorganic interfaces to discover new materials: insights, comparisons to experiment, challenges, and opportunities, Chem. Soc. Rev. 45 (2016) 412–448.
[48] A.G. Kalinichev, R.J. Kirkpatrick, Molecular dynamics modeling of chloride binding to the surfaces of calcium hydroxide, hydrated calcium aluminate, and calcium silicate phases, Chem. Mater. 14 (2002) 3539–3549.
[49] R.K. Mishra, R.J. Flatt, H. Heinz, Force field for tricalcium silicate and insight into nanoscale properties: cleavage, initial hydration, and adsorption of organic molecules, J. Phys. Chem. C 117 (2013) 10417–10432.
[50] R.K. Mishra, L. Fernandez-Carrasco, R.J. Flatt, H. Heinz, A force field for tricalcium aluminate to characterize surface properties, initial hydration, and organically modified interfaces in atomic resolution, Dalton Trans. 43 (2014) 10602–10616.
[51] H. Heinz, T.-J. Lin, R.K. Mishra, F.S. Emami, Thermodynamically consistent force fields for the assembly of inorganic, organic, and biological nanostructures: the INTERFACE force field, Langmuir 29 (2013) 1754–1765.
[52] R.J. Pellenq, A. Kushima, R. Shahsavari, K.J. Van Vliet, M.J. Buehler, S. Yip, F.J. Ulm, A realistic molecular model of cement hydrates, Proc. Natl. Acad. Sci. U. S. A. 106 (2009) 16102–16107.
[53] J.P. Allen, W. Gren, M. Molinari, C. Arrouvel, F. Maglia, S.C. Parker, Atomistic modelling of adsorption and segregation at inorganic solid interfaces, Mol. Simul. 35 (2009) 584–608.
[54] P. Faucon, J.M. Delaye, J. Virlet, J.F. Jacquinot, F. Adenot, Study of the structural properties of the C-S-H(I) by molecular dynamics simulation, Cem. Concr. Res. 27 (1997) 1581–1590.
[55] P.V. Coveney, W. Humphries, Molecular modelling of the mechanism of action of phosphonate retarders on hydrating cements, J. Chem. Soc. Faraday Trans. 92 (1996) 831–841.
[56] S.V. Churakov, C. Labbez, Thermodynamics and molecular mechanism of Al incorporation in calcium silicate hydrates, J. Phys. Chem. C 121 (2017) 4412–4419.
[57] L. Nicoleau, E. Schreiner, A. Nonat, Ion-specific effects influencing the dissolution of tricalcium silicate, Cem. Concr. Res. 59 (2014) 118–138.
[58] H. Manzano, E. Durgun, I. López-Arbeloa, J.C. Grossman, Insight on tricalcium silicate hydration and dissolution mechanism from molecular simulations, ACS Appl. Mater. Interfaces 7 (2015) 14726–14733.
[59] G. Kovačević, B. Persson, L. Nicoleau, A. Nonat, V. Veryazov, Atomistic modeling of crystal structure of Ca1.67SiHx, Cem. Concr. Res. 67 (2015) 197–203.
[60] I.G. Richardson, The importance of proper crystal-chemical and geometrical reasoning demonstrated using layered single and double hydroxides, Acta Crystallogr. Sect. B: Struct. Sci. Cryst. Eng. Mater. 69 (2013) 150–162.
[61] J.D. Gale, A.L. Rohl, The general utility lattice program (GULP), Mol. Simul. 29 (2003) 291–341.
[62] A.C. Van Duin, S. Dasgupta, F. Lorant, W.A. Goddard, ReaxFF: a reactive force field for hydrocarbons, J. Phys. Chem. A 105 (2001) 9396–9409.
[63] A.K. Rappé, C.J. Casewit, K. Colwell, W. Goddard Iii, W. Skiff, UFF, a full periodic table force field for molecular mechanics and molecular dynamics simulations, J. Am. Chem. Soc. 114 (1992) 10024–10035.
[64] H. Heinz, U.W. Suter, Atomic charges for classical simulations of polar systems, J. Phys. Chem. B 108 (2004) 18341–18352.
[65] H. Heinz, C. Pramanik, O. Heinz, Y. Ding, R.K. Mishra, D. Marchon, R.J. Flatt, I. Estrela-Lopis, J. Llop, S. Moya, R.F. Ziolo, Nanoparticle decoration with surfactants: molecular interactions, assembly, and applications, Surf. Sci. Rep. 72 (2017) 1–58.
[66] D. Tavakoli, A. Tarighat, Molecular dynamics study on the mechanical properties of Portland cement clinker phases, Comput. Mater. Sci. 119 (2016) 65–73.
[67] A. Al-Ostaz, W. Wu, A.H.D. Cheng, C.R. Song, A molecular dynamics and micromechanics study on the mechanical properties of major constituents of hydrated cement, Compos. Part B 41 (2010) 543–549.
[68] E.B. Tadmor, R. Elliott, J. Sethna, R. Miller, C. Becker, Knowledgebase of Interatomic Models (KIM), (2011).
[69] C.A. Becker, F. Tavazza, Z.T. Trautt, R.A.B. de Macedo, Considerations for choosing and using force fields and interatomic potentials in materials science and engineering, Curr. Opinion Solid State Mater. Sci. 17 (2013) 277–283.
[70] http://flask.pocoo.org/.
[71] M. Bayer, Sqlalchemy-The Database Toolkit for Python, URL http://www.sqlalchemy.org/. Accessed on the 13th of November, (2012).
[72] J. Gruber, Daring Fireball: Markdown Syntax Documentation, December (2004).
[73] https://www.mathjax.org/.
[74] A.G. Kalinichev, P. Padma Kumar, R. James Kirkpatrick, Molecular dynamics computer simulations of the effects of hydrogen bonding on the properties of layered double hydroxides intercalated with organic acids, Philos. Mag. 90 (2010) 2475–2488.
[75] A.G. Kalinichev, J.W. Wang, R.J. Kirkpatrick, Molecular dynamics modeling of the structure, dynamics and energetics of mineral-water interfaces: application to cement materials, Cem. Concr. Res. 37 (2007) 337–347.
[76] A.G. Kalinichev, Molecular structure and dynamics of nano-confined water: computer simulations of aqueous species in clay, cement, and polymer membranes, in: L. Mercury, N. Tas, M. Zilberbrand (Eds.), Transport and Reactivity of Solutions in Confined Hydrosystems, Springer Netherlands, Dordrecht, 2014, pp. 103–115.
[77] H. Heinz, H. Koerner, K.L. Anderson, R.A. Vaia, B.L. Farmer, Force field for mica-type silicates and dynamics of octadecylammonium chains grafted to montmorillonite, Chem. Mater. 17 (2005) 5658–5669.
[78] H. Heinz, H.J. Castelijns, U.W. Suter, Structure and phase transitions of alkyl chains on mica, J. Am. Chem. Soc. 125 (2003) 9500–9510.
[79] A.G. Kalinichev, R.J. Kirkpatrick, R.T. Cygan, Molecular modeling of the structure and dynamics of the interlayer and surface species of mixed-metal layered hydroxides: chloride and water in hydrocalumite (Friedel's salt), Am. Mineral. 85 (2000) 1046–1052.
[80] S.L. Teich-McGoldrick, J.A. Greathouse, R.T. Cygan, Molecular dynamics simulations of uranyl adsorption and structure on the basal surface of muscovite, Mol. Simul. 40 (2014) 610–617.
[81] H.J.C. Berendsen, J.P.M. Postma, W.F. van Gunsteren, J. Hermans, Interaction models for water in relation to protein hydration, in: B. Pullman (Ed.), Intermolecular Forces: Proceedings of the Fourteenth Jerusalem Symposium on Quantum Chemistry and Biochemistry Held in Jerusalem, Israel, April 13–16, 1981, Springer Netherlands, Dordrecht, 1981, pp. 331–342.
[82] O. Teleman, B. Jönsson, S. Engström, A molecular dynamics simulation of a water model with intramolecular degrees of freedom, Mol. Phys. 60 (1987) 193–203.
[83] H. Heinz, R.A. Vaia, B.L. Farmer, R.R. Naik, Accurate simulation of surfaces and interfaces of face-centered cubic metals using 12 – 6 and 9 – 6 Lennard-Jones potentials, J. Phys. Chem. C 112 (2008) 17281–17290.
[84] F.S. Emami, V. Puddu, R.J. Berry, V. Varshney, S.V. Patwardhan, C.C. Perry, H. Heinz, Force field and a surface model database for silica to simulate interfacial properties in atomic resolution, Chem. Mater. 26 (2014) 2647–2658.
[85] E. Pustovgar, R.K. Mishra, M. Palacios, J.-B. d'Espinose de Lacaillerie, T. Matschei, A.S. Andreev, H. Heinz, R. Verel, R.J. Flatt, Influence of aluminates on the hydration kinetics of tricalcium silicate, Cem. Concr. Res. 100 (2017) 245–262.
[86] H. Sun, Force field for computation of conformational energies, structures, and vibrational frequencies of aromatic polyesters, J. Comput. Chem. 15 (1994) 752–768.
[87] H. Sun, Ab-initio calculations and force-field development for computer-simulation of polysilanes, Macromolecules 28 (1995) 701–712.
[88] H. Sun, S.J. Mumby, J.R. Maple, A.T. Hagler, An ab-initio CFF93 all-atom force field for polycarbonates, J. Am. Chem. Soc. 116 (1994) 2978–2987.
[89] H. Sun, COMPASS: an ab initio force-field optimized for condensed-phase applications - overview with details on alkane and benzene compounds, J. Phys. Chem. B 102 (1998) 7338–7364.
[90] A.D. MacKerell Jr., D. Bashford, M. Bellott, R.L. Dunbrack Jr., J.D. Evanseck, M.J. Fields, S. Fischer, J. Gao, H. Guo, S. Ha, D. Joseph-McCarthy, L. Kuchnir, K. Kuczera, F.T.K. Lau, C. Mattos, S. Michnick, T. Ngo, D.T. Nguyen, B. Prodhom, W.E. Reiher III, B. Roux, M. Schlenkrich, J.C. Smith, R. Stote, J. Straub, D. Watanabe, J. Wiórkiewicz-Kuczera, D. Yin, M. Karplus, All-atom empirical potential for molecular modeling and dynamics studies of proteins, J. Phys. Chem. B 102 (1998) 3586–3616.
[91] J.M. Wang, R.M. Wolf, J.W. Caldwell, P.A. Kollman, D.A. Case, Development and testing of a general amber force field, J. Comput. Chem. 25 (2004) 1157–1174.
[92] B. Hess, C. Kutzner, D. Van Der Spoel, E. Lindahl, GROMACS 4: algorithms for highly efficient, load-balanced, and scalable molecular simulation, J. Chem. Theory Comput. 4 (2008) 435–447.
[93] W.L. Jorgensen, D.S. Maxwell, J. TiradoRives, Development and testing of the OPLS all-atom force field on conformational energetics and properties of organic liquids, J. Am. Chem. Soc. 118 (1996) 11225–11236.
[94] T.-J. Lin, H. Heinz, Accurate force field parameters and pH resolved surface models for hydroxyapatite to understand structure, mechanics, hydration, and biological interfaces, J. Phys. Chem. C 120 (2016) 4975–4992.
[95] T.A. Halgren, Merck molecular force field. I. Basis, form, scope, parameterization, and performance of MMFF94, J. Comput. Chem. 17 (1996) 490–519.
[96] P. Dauber-Osguthorpe, V.A. Roberts, D.J. Osguthorpe, J. Wolff, M. Genest, A.T. Hagler, Structure and Energetics of Ligand Binding to Proteins: *Escherichia coli* Dihydrofolate Reductase-trimethoprim, a Drug-receptor System, Proteins: Struct., Funct., Genet, 4 (1988), pp. 31–47.
[97] K.C. Gross, P.G. Seybold, C.M. Hadad, Comparison of different atomic charge schemes for predicting pKa variations in substituted anilines and phenols*, Int. J. Quantum Chem. 90 (2002) 445–458.
[98] F.S. Emami, V. Puddu, R.J. Berry, V. Varshney, S.V. Patwardhan, C.C. Perry, H. Heinz, Prediction of specific biomolecule adsorption on silica surfaces as a function of pH and particle size, Chem. Mater. 26 (2014) 5725–5734.
[99] N.M. Bedford, H. Ramezani-Dakhel, J.M. Slocik, B.D. Briggs, Y. Ren, A.I. Frenkel, V. Petkov, H. Heinz, R.R. Naik, M.R. Knecht, Elucidation of peptide-directed palladium surface structure for biologically tunable nanocatalysts, ACS Nano 9 (2015) 5082–5092.
[100] C.L. Freeman, J.H. Harding, D.J. Cooke, J.A. Elliott, J.S. Lardge, D.M. Duffy, New forcefields for modeling biomineralization processes, J. Phys. Chem. C 111 (2007) 11943–11951.
[101] K.P. Schröder, J. Sauer, M. Leslie, C. Richard, A. Catlow, J.M. Thomas, Bridging hydrodyl groups in zeolitic catalysts: a computer simulation of their structure, vibrational properties and acidity in protonated faujasites (HY zeolites), Chem. Phys. Lett. 188 (1992) 320–325.
[102] G.V. Lewis, C.R.A. Catlow, Potential Models for Ionic Oxides, (1985), pp. 1149–1161.
[103] J.L.F. Abascal, C. Vega, A General Purpose Model for the Condensed Phases of Water: TIP4P/2005, The Journal of chemical physics (2005).
[104] N. de Leeuw, S. Parker, Effect of chemisorption and physisorption of water on the surface structure and stability of alpha-alumina, J. Am. Ceram. Soc. 16 (1999) 3209–3216.
[105] G.W. Watson, E.T. Kelsey, N.H. de Leeuw, D.J. Harris, S.C. Parker, Atomistic simulation of dislocations, surfaces and interfaces in MgO, J. Chem. Soc. Faraday Trans. 92 (1996) 433–438.

[106] S. Galmarini, P. Bowen, Atomistic simulation of the adsorption of calcium and hydroxyl ions onto portlandite surfaces - towards crystal growth mechanisms, Cem. Concr. Res. 81 (2016) 16–23.
[107] S.C. Galmarini, Atomistic Simulation of Cementitious Systems, EPFL (2013).
[108] A.C.T. van Duin, A. Strachan, S. Stewman, Q. Zhang, X. Xu, W.A. Goddard, ReaxFFSiO reactive force field for silicon and silicon oxide systems, J. Phys. Chem. A 107 (2003) 3803–3811.
[109] A.D. McNaught, A. Wilkinson, Compendium of Chemical Terminology, IUPAC recommendations (1997).
[110] P. Bultinck, W. Langenaeker, P. Lahorte, F. De Proft, P. Geerlings, M. Waroquier, J. Tollenaere, The electronegativity equalization method I: parametrization and validation for atomic charge calculations, J. Phys. Chem. A 106 (2002) 7887–7894.
[111] R. Mortier, C. Vandecasteele, J. Hoste, F. Den Hartog, Determination of boron in magnesium oxide by charged particle activation analysis, J. Radioanal. Nucl. Chem. 105 (1986) 47–56.
[112] J. Yeon, A.C. van Duin, ReaxFF molecular dynamics simulations of hydroxylation kinetics for amorphous and nano-silica structure, and its relations with atomic strain energy, J. Phys. Chem. C 120 (2015) 305–317.
[113] T.P. Senftle, A.C. van Duin, M.J. Janik, Determining in situ phases of a nanoparticle catalyst via grand canonical Monte Carlo simulations with the ReaxFF potential, Catal. Commun. 52 (2014) 72–77.
[114] S.J. Plimpton, A.P. Thompson, Computational aspects of many-body potentials, MRS Bull. 37 (2012) 513–521.
[115] K. Chenoweth, A.C. Van Duin, S. Dasgupta, W.A. Goddard Iii, Initiation mechanisms and kinetics of pyrolysis and combustion of JP-10 hydrocarbon jet fuel, J. Phys. Chem. A 113 (2009) 1740–1746.
[116] E.C. Neyts, Y. Shibuta, A.C. van Duin, A. Bogaerts, Catalyzed growth of carbon nanotube with definable chirality by hybrid molecular dynamics − force biased Monte Carlo simulations, ACS Nano 4 (2010) 6665–6672.
[117] X. Huang, H. Yang, W. Liang, M. Raju, M. Terrones, V.H. Crespi, A.C. Van Duin, S. Zhang, Lithiation induced corrosive fracture in defective carbon nanotubes, Appl. Phys. Lett. 103 (2013) 153901.
[118] K. Chenoweth, A.C. Van Duin, W.A. Goddard, ReaxFF reactive force field for molecular dynamics simulations of hydrocarbon oxidation, J. Phys. Chem. A 112 (2008) 1040–1053.
[119] D. Raymand, A.C. van Duin, W.A. Goddard III, K. Hermansson, D. Spångberg, Hydroxylation structure and proton transfer reactivity at the zinc oxide − water interface, J. Phys. Chem. C 115 (2011) 8573–8579.
[120] T.P. Senftle, S. Hong, M.M. Islam, S.B. Kylasa, Y. Zheng, Y.K. Shin, C. Junkermeier, R. Engel-Herbert, M.J. Janik, H.M. Aktulga, The ReaxFF reactive force-field: development, applications and future directions, Comput. Mater. 2 (2016) 15011.
[121] A.V. Akimov, O.V. Prezhdo, Large-scale computations in chemistry: a bird's eye view of a vibrant field, Chem. Rev. 115 (2015) 5797–5890.
[122] J.C. Fogarty, H.M. Aktulga, A.Y. Grama, A.C. Van Duin, S.A. Pandit, A reactive molecular dynamics simulation of the silica-water interface, J. Chem. Phys. 132 (2010) 174704.
[123] H. Manzano, S. Moeini, F. Marinelli, A.C. Van Duin, F.-J. Ulm, R.J.-M. Pellenq, Confined water dissociation in microporous defective silicates: mechanism, dipole distribution, and impact on substrate properties, J. Am. Chem. Soc. 134 (2012) 2208–2215.
[124] H. Manzano, E. Masoero, I. Lopez-Arbeloa, H.M. Jennings, Mechanical behaviour of ordered and disordered calcium silicate hydrates under shear strain studied by atomic scale simulations, Mechanics and Physics of Creep, Shrinkage, and Durability of Concrete: A Tribute to Zdeněk P. Bažant, ASCE, 2013, pp. 86–97.
[125] M.A. Qomi, K.J. Krakowiak, M. Bauchy, K. Stewart, R. Shahsavari, D. Jagannathan, D.B. Brommer, A. Baronnet, M.J. Buehler, S. Yip, Combinatorial Molecular Optimization of Cement Hydrates, Nature Communications, 5 (2014).
[126] D. Hou, Y. Zhu, Y. Lu, Z. Li, Mechanical properties of calcium silicate hydrate (C–S–H) at nano-scale: a molecular dynamics study, Mater. Chem. Phys. 146 (2014) 503–511.
[127] M. Bauchy, M.J. Abdolhosseini Qomi, C. Bichara, F.-J. Ulm, R.J.-M. Pellenq, Nanoscale structure of cement: viewpoint of rigidity theory, J. Phys. Chem. C 118 (2014) 12485–12493.
[128] M. Bauchy, M.A. Qomi, F.-J. Ulm, R.-M. Pellenq, Order and disorder in calcium–silicate–hydrate, J. Chem. Phys. 140 (2014) 214503.
[129] D. Hou, Z. Li, T. Zhao, P. Zhang, Water transport in the nano-pore of the calcium silicate phase: reactivity, structure and dynamics, Phys. Chem. Chem. Phys. 17 (2015) 1411–1423.
[130] M.J.A. Qomi, M. Bauchy, F.-J. Ulm, R.J.-M. Pellenq, Anomalous composition-dependent dynamics of nanoconfined water in the interlayer of disordered calcium-silicates, J. Chem. Phys. 140 (2014) 054515.
[131] M.C. Pitman, A.C. Van Duin, Dynamics of confined reactive water in smectite clay–zeolite composites, J. Am. Chem. Soc. 134 (2012) 3042–3053.
[132] S.E. Moghaddam, V. Hejazi, S.H. Hwang, S. Sreenivasan, J. Miller, B. Shi, S. Zhao, I. Rusakova, A.R. Alizadeh, K.H. Whitmire, R. Shahsavari, Morphogenesis of cement hydrate, J. Mater. Chem. A 5 (2017) 3798–3811.
[133] J.D. Gale, Empirical potential derivation for ionic materials, Philos. Mag. B 73 (1996) 3–19.
[134] E. Bonaccorsi, S. Merlino, A.R. Kampf, The crystal structure of tobermorite 14 Å (plombierite), a C-S-H phase, J. Am. Ceram. Soc. 88 (2005) 505–512.
[135] S. Hamid, The crystal structure of the 11 Å natural tobermorite $Ca_2{\cdot}25[Si_3O_7{\cdot}5(OH)_{1.5}]{\cdot}1H_2O$, Z. Krist.-Cryst. Mater. 154 (1981) 189–198.
[136] R. Shahsavari, L. Chen, L. Tao, Edge dislocations in dicalcium silicates: experimental observations and atomistic analysis, Cem. Concr. Res. 90 (2016) 80–88.
[137] B. Van Beest, G.J. Kramer, R. Van Santen, Force fields for silicas and aluminophosphates based on ab initio calculations, Phys. Rev. Lett. 64 (1990) 1955.
[138] R. Shahsavari, M.J. Buehler, R.J.M. Pellenq, F.J. Ulm, First-principles study of elastic constants and interlayer interactions of complex hydrated oxides: case study of tobermorite and jennite, J. Am. Ceram. Soc. 92 (2009) 2323–2330.
[139] C.J. O'Brien, J.A. Greathouse, C.M. Tenney, Dissociation of sarin on a cement analogue surface: effects of humidity and confined geometry, J. Phys. Chem. C 120 (2016) 28100–28109.
[140] S.M. Mutisya, J.M. de Almeida, C.R. Miranda, Molecular simulations of cement based materials: a comparison between first principles and classical force field calculations, Comput. Mater. Sci. 138 (2017) 392–402.
[141] R.T. Cygan, J.A. Greathouse, H. Heinz, A.G. Kalinichev, Molecular models and simulations of layered materials, J. Mater. Chem. 19 (2009) 2470–2481.
[142] R.J. Kirkpatrick, A.G. Kalinichev, X. Hou, L. Struble, Experimental and molecular dynamics modeling studies of interlayer swelling: water incorporation in kanemite and ASR gel, Mater. Struct. 38 (2005) 449–458.
[143] R.J. Kirkpatrick, A.G. Kalinichev, G.M. Bowers, A.Ö. Yazaydin, M. Krishnan, M. Saharay, C.P. Morrow, NMR and computational molecular modeling studies of mineral surfaces and interlayer galleries: a review, Am. Mineral. 100 (2015) 1341–1354.
[144] S. Plimpton, Fast parallel algorithms for short-range molecular dynamics, J. Comput. Phys. 117 (1995) 1–19.
[145] I.T. Todorov, W. Smith, K. Trachenko, M.T. Dove, DL_POLY_3: new dimensions in molecular dynamics simulations via massive parallelism, J. Mater. Chem. 16 (2006) 1911–1918.
[146] J.C. Phillips, R. Braun, W. Wang, J. Gumbart, E. Tajkhorshid, E. Villa, C. Chipot, R.D. Skeel, L. Kalé, K. Schulten, Scalable molecular dynamics with NAMD, J. Comput. Chem. 26 (2005) 1781–1802.
[147] M.G. Martin, MCCCS Towhee: a tool for Monte Carlo molecular simulation, Mol. Simul. 39 (2013) 1212–1222.
[148] P.P. Kumar, A.G. Kalinichev, R.J. Kirkpatrick, Molecular dynamics simulation of the energetics and structure of layered double hydroxides intercalated with carboxylic acids, J. Phys. Chem. C 111 (2007) 13517–13523.
[149] F. Module, Material Studio 6.0, Accelrys Inc., San Diego, CA, 2011.
[150] B. Hess, C. Kutzner, D. van der Spoel, E. Lindahl, GROMACS 4: algorithms for highly efficient, load-balanced, and scalable molecular simulation, J. Chem. Theory Comput. 4 (2008) 435–447.
[151] W. Mumme, Crystal structure of tricalcium silicate from a Portland cement clinker and its application to quantitative XRD analysis, Neues Jb. Mineral. Monat. 4 (1995) 145–160.
[152] L. Desgranges, D. Grebille, G. Calvarin, G. Chevrier, N. Floquet, J.-C. Niepce, Hydrogen thermal motion in calcium hydroxide: $Ca(OH)_2$, Acta Crystallogr. B 49 (1993) 812–817.
[153] S. Merlino, E. Bonaccorsi, T. Armbruster, The real structure of tobermorite 11 Å, Eur. J. Mineral. 13 (2001) 577–590.
[154] S. Galmarini, A. Kunhi Mohamed, P. Bowen, Atomistic Simulations of Silicate Species Interaction with Portlandite Surfaces, The Journal of Physical Chemistry C 120 (2016) 22407–22413.
[155] H. Manzano, J. Dolado, A. Ayuela, Elastic properties of the main species present in Portland cement pastes, Acta Mater. 57 (2009) 1666–1674.
[156] E. Durgun, H. Manzano, P. Kumar, J.C. Grossman, The characterization, stability, and reactivity of synthetic calcium silicate surfaces from first principles, J. Phys. Chem. C 118 (2014) 15214–15219.
[157] H.M. Aktulga, J.C. Fogarty, S.A. Pandit, A.Y. Grama, Parallel reactive molecular dynamics: numerical methods and algorithmic techniques, Parallel Comput. 38 (2012) 245–259.
[158] P. Baranek, A. Lichanot, R. Orlando, R. Dovesi, Structural and vibrational properties of solid $Mg(OH)_2$ and $Ca(OH)_2$ – performances of various Hamiltonians, Chem. Phys. Lett. 340 (2001) 362–369.
[159] P.J.M. Monteiro, C.T. Chang, The elastic moduli of calcium hydroxide, Cem. Concr. Res. 25 (1995) 1605–1609.
[160] F. Holuj, M. Drozdowski, M. Czajkowski, Brillouin spectrum of $Ca(OH)_2$, Solid State Commun. 56 (1985) 1019–1021.
[161] A. Boumiz, D. Sorrentino, C. Vernet, F.C. Tenoudji, A. Nonat, Modelling the development of the elastic moduli as a function of the hydration degree of cement pastes and mortars, 2nd International Rilem Workshop on Hydration and Setting: Why Does Cement Set, 2000, pp. 295–316.
[162] K. Velez, S. Maximilien, D. Damidot, G. Fantozzi, F. Sorrentino, Determination by nanoindentation of elastic modulus and hardness of pure constituents of Portland cement clinker, Cem. Concr. Res. 31 (2001) 555–561.
[163] J. Moon, Experimental and Theoretical Studies on Mechanical Properties of Complex Oxides in Concrete, UC Berkeley, 2013.
[164] J.E. Oh, S.M. Clark, H.-R. Wenk, P.J. Monteiro, Experimental determination of bulk modulus of 14 Å tobermorite using high pressure synchrotron X-ray diffraction, Cem. Concr. Res. 42 (2012) 397–403.
[165] S. Brunauer, D.L. Kantro, C.H. Weise, The surface energies of calcium oxide and calcium hydroxide, Can. J. Chem. 34 (1956) 729–742.
[166] D.H. Klein, M.D. Smith, Homogeneous nucleation of calcium hydroxide, Talanta 15 (1968) 229–231.
[167] C. Estrela, C.R.D.A. Estrela, L.F. Guimarães, R.S. Silva, J.D. Pécora, Surface tension of calcium hydroxide associated with different substances, J. Appl. Oral Sci. 13 (2005) 152–156.
[168] P. Juilland, E. Gallucci, R.J. Flatt, K.L. Scrivener, Reply to the discussion by E. Gartner of the paper "Dissolution theory applied to the induction period in alite hydration", Cem. Concr. Res. 41 (2011) 563–564.
[169] S. Brunauer, D.L. Kantro, C.H. Weise, The surface energy of tobermorite, Can. J.

Chem. 37 (1959) 714–724.
[170] S.V. Churakov, C. Labbez, L. Pegado, M. Sulpizi, Intrinsic acidity of surface sites in calcium silicate hydrates and its implication to their electrokinetic properties, J. Phys. Chem. C 118 (2014) 11752–11762.
[171] T. Verstraelen, V.V. Speybroeck, M. Waroquier, The electronegativity equalization method and the split charge equilibration applied to organic systems: parametrization, validation, and comparison, J. Chem. Phys. 131 (2009) 044127.
[172] J.J. Beaudoin, L. Raki, R. Alizadeh, A 29Si MAS NMR study of modified C–S–H nanostructures, Cem. Concr. Compos. 31 (2009) 585–590.
[173] S. Kerisit, C. Liu, E.S. Ilton, Molecular dynamics simulations of the orthoclase (001)- and (010)-water interfaces, Geochim. Cosmochim. Acta 72 (2008) 1481–1497.
[174] J.A. Greathouse, J.S. Durkin, J.P. Larentzos, R.T. Cygan, Implementation of a Morse potential to model hydroxyl behavior in phyllosilicates, J. Chem. Phys. 130 (2009) 134713.
[175] E. Ferrage, B.A. Sakharov, L.J. Michot, A. Delville, A. Bauer, B. Lanson, S. Grangeon, G. Frapper, M. Jiménez-Ruiz, G.J. Cuello, Hydration properties and interlayer organization of water and ions in synthetic Na-smectite with tetrahedral layer charge. Part 2. Toward a precise coupling between molecular simulations and diffraction data, J. Phys. Chem. C 115 (2011) 1867–1881.
[176] M. Szczerba, A. Kugliewicz, A. Derkowski, V. Gionis, G.D. Chryssikos, A. Kalinichev, Structure and dynamics of water-smectite interfaces: hydrogen bonding and the origin of the sharp O-Dw/O-Hw infrared band from molecular simulations, Clay Clay Miner. 64 (2016) 452–471.
[177] M. Pouvreau, J.A. Greathouse, R.T. Cygan, A.G. Kalinichev, Structure of hydrated gibbsite and brucite edge surfaces: DFT results and further development of the ClayFF classical force field with metal–O–H angle bending terms, J. Phys. Chem. C 121 (2017) 14757–14771.
[178] H. Heinz, Adsorption of biomolecules and polymers on silicates, glasses, and oxides: mechanisms, predictions, and opportunities by molecular simulation, Curr. Opin. Chem. Eng. 11 (2016) 34–41.
[179] R.K. Mishra, M. Weibel, T. Müller, H. Heinz, R.J. Flatt, Energy-effective grinding of inorganic solids using organic additives, CHIMIA Int. J. Chem. 71 (2017) 451–460.
[180] Y.-T. Fu, H. Heinz, Cleavage energy of alkylammonium-modified montmorillonite and relation to exfoliation in nanocomposites: influence of cation density, head group structure, and chain length, Chem. Mater. 22 (2010) 1595–1605.
[181] H. Heinz, R.A. Vaia, B.L. Farmer, Interaction energy and surface reconstruction between sheets of layered silicates, J. Chem. Phys. 124 (2006) 224713.
[182] J.P. Korb, P.J. McDonald, L. Monteilhet, A.G. Kalinichev, R.J. Kirkpatrick, Comparison of proton field-cycling relaxometry and molecular dynamics simulations for proton–water surface dynamics in cement-based materials, Cem. Concr. Res. 37 (2007) 348–350.
[183] A. Alex, A.K. Nagesh, P. Ghosh, Surface dissimilarity affects critical distance of influence for confined water, RSC Adv. 7 (2017) 3573–3584.
[184] R.K. Mishra, Simulation of Interfaces in Construction Materials: Tricalcium Silicate, Gypsum, and Organic Modifiers, The University of Akron, 2012.
[185] R.K. Mishra, H. Heinz, J. Zimmermann, T. Müller, R.J. Flatt, Understanding the Effectiveness of Polycarboxylates as Grinding Aids, ACI Special Publication 288 (2012), pp. 1–15.
[186] F. Begarin, S. Garrault, A. Nonat, L. Nicoleau, Hydration of alite containing aluminium, Adv. Appl. Ceram. 110 (2011) 127–130.
[187] A. Quennoz, K.L. Scrivener, Interactions between alite and C3A-gypsum hydrations in model cements, Cem. Concr. Res. 44 (2013) 46–54.
[188] P. Suraneni, R.J. Flatt, Use of micro-reactors to obtain new insights into the factors influencing tricalcium silicate dissolution, Cem. Concr. Res. 78 (Part B) (2015) 208–215.
[189] M.E. Tadros, J.A.N. Skalny, R.S. Kalyoncu, Early hydration of tricalcium silicate, J. Am. Ceram. Soc. 59 (1976) 344–347.
[190] J.F. Young, H.S. Tong, R.L. Berger, Compositions of solutions in contact with hydrating tricalcium silicate pastes, J. Am. Ceram. Soc. 60 (1977) 193–198.
[191] I. Odler, H. Dörr, Early hydration of tricalcium silicate II. The induction period, Cem. Concr. Res. 9 (1979) 277–284.
[192] A. Kumar, B.J. Walder, A. Kunhi Mohamed, A. Hofstetter, B. Srinivasan, A.J. Rossini, K. Scrivener, L. Emsley, P. Bowen, The Atomic-Level Structure of Cementitious Calcium Silicate Hydrate, J. Phys. Chem. C 121 (2017) 17188–17196.
[193] L. Nicoleau, A. Nonat, D. Perrey, The di- and tricalcium silicate dissolutions, Cem. Concr. Res. 47 (2013) 14–30.
[194] J.W. Bullard, A determination of hydration mechanisms for tricalcium silicate using a kinetic cellular automaton model, J. Am. Ceram. Soc. 91 (2008) 2088–2097.
[195] D. Jansen, S.T. Bergold, F. Goetz-Neunhoeffer, J. Neubauer, The hydration of alite: a time-resolved quantitative X-ray diffraction approach using the G-factor method compared with heat release, J. Appl. Crystallogr. 44 (2011) 895–901.
[196] E. Durgun, H. Manzano, R.J.M. Pellenq, J.C. Grossman, Understanding and controlling the reactivity of the calcium silicate phases from first principles, Chem. Mater. 24 (2012) 1262–1267.
[197] J. Huang, B. Wang, Y. Yu, L. Valenzano, M. Bauchy, G. Sant, Electronic origin of doping-induced enhancements of reactivity: case study of tricalcium silicate, J. Phys. Chem. C 119 (2015) 25991–25999.
[198] K. Saritas, C. Ataca, J.C. Grossman, Predicting electronic structure in tricalcium silicate phases with impurities using first-principles, J. Phys. Chem. C 119 (2015) 5074–5079.
[199] Q. Wang, F. Li, X. Shen, W. Shi, X. Li, Y. Guo, S. Xiong, Q. Zhu, Relation between reactivity and electronic structure for α'L-, β- and γ-dicalcium silicate: a first-principles study, Cem. Concr. Res. 57 (2014) 28–32.
[200] H. Manzano, J.S. Dolado, A. Ayuela, Structural, mechanical, and reactivity properties of tricalcium aluminate using first-principles calculations, J. Am. Ceram. Soc. 92 (2009) 897–902.
[201] Q. Wang, H. Manzano, Y. Guo, I. Lopez-Arbeloa, X. Shen, Hydration mechanism of reactive and passive dicalcium silicate polymorphs from molecular simulations, J. Phys. Chem. C 119 (2015) 19869–19875.
[202] B. Fubini, V. Bolis, M. Bailes, F.S. Stone, The reactivity of oxides with water vapor, Solid State Ionics 32 (1989) 258–272.
[203] J. Cot-Gores, A. Castell, L.F. Cabeza, Thermochemical energy storage and conversion: a-state-of-the-art review of the experimental research under practical conditions, Renew. Sust. Energ. Rev. 16 (2012) 5207–5224.
[204] K. Kudłacz, C. Rodriguez-Navarro, The mechanism of vapor phase hydration of calcium oxide: implications for CO_2 capture, Environ. Sci. Technol. 48 (2014) 12411–12418.
[205] H.S. Craft, R. Collazo, M.D. Losego, Z. Sitar, J.-P. Maria, Surface water reactivity of polycrystalline MgO and CaO films investigated using X-ray photoelectron spectroscopy, J. Vac. Sci. Technol. A 26 (2008) 1507–1510.
[206] S.A. Sheikholeslam, H. Manzano, C. Grecu, A. Ivanov, Reduced hydrogen diffusion in strained amorphous SiO_2: understanding ageing in MOSFET devices, J. Mater. Chem. C 4 (2016) 8104–8110.
[207] R. Paolo, D.G. Julian, B. Giovanni, Reactive force field simulation of proton diffusion in BaZrO 3 using an empirical valence bond approach, J. Phys. Condens. Matter 23 (2011) 334213.
[208] W.H. Casey, C. Ludwig, The mechanism of dissolution of oxide minerals, Nature 381 (1996) 506–509.
[209] M. Youssef, R.J.M. Pellenq, B. Yildiz, Glassy nature of water in an ultraconfining disordered material: the case of calcium − silicate − hydrate, J. Am. Chem. Soc. 133 (2011) 2499–2510.
[210] P.A. Bonnaud, Q. Ji, B. Coasne, R.J.M. Pellenq, K.J. Van Vliet, Thermodynamics of water confined in porous calcium-silicate-hydrates, Langmuir 28 (2012) 11422–11432.
[211] P.A. Bonnaud, Q. Ji, K.J. Van Vliet, Effects of elevated temperature on the structure and properties of calcium-silicate-hydrate gels: the role of confined water, Soft Matter 9 (2013) 6418–6429.
[212] Q. Ji, R.J.M. Pellenq, K.J. Van Vliet, Comparison of computational water models for simulation of calcium–silicate–hydrate, Comput. Mater. Sci. 53 (2012) 234–240.
[213] N. Sakhavand, Mechanics of Platelet-Matrix Composites across Scales: Theory, Multiscale Modeling, and 3D Fabrication, PhD Thesis (2015).
[214] D. Hou, J. Zhang, Z. Li, Y. Zhu, Uniaxial tension study of calcium silicate hydrate (C–S–H): structure, dynamics and mechanical properties, Mater. Struct. 48 (2015) 3811–3824.
[215] S. Jalilvand, R. Shahsavari, Molecular mechanistic origin of nanoscale contact, friction, and scratch in complex particulate systems, ACS Appl. Mater. Interfaces 7 (2015) 3362–3372.
[216] N. Zhang, R. Shahsavari, Balancing strength and toughness of calcium-silicate-hydrate via random nanovoids and particle inclusions: atomistic modeling and statistical analysis, J. Mech. Phys. Solids 96 (2016) 204–222.
[217] L. Tao, R. Shahsavari, Diffusive, Displacive Deformations and Local Phase Transformation Govern the Mechanics of Layered Crystals: The Case Study of Tobermorite, Nature Scientific Reports, 7 (2017) 5907.
[218] N. Zhang, P. Carrez, R. Shahsavari, Screw-dislocation-induced strengthening–toughening mechanisms in complex layered materials: the case study of tobermorite, ACS Appl. Mater. Interfaces 9 (2017) 1496–1506.
[219] M.J. Abdolhosseini Qomi, F.-J. Ulm, R.J.M. Pellenq, Physical origins of thermal properties of cement paste, Phys. Rev. Appl. 3 (2015) 064010.
[220] S. Hajilar, B. Shafei, Assessment of structural, thermal, and mechanical properties of portlandite through molecular dynamics simulations, J. Solid State Chem. 244 (2016) 164–174.
[221] M.A. Rafiee, T.N. Narayanan, D.P. Hashim, N. Sakhavand, R. Shahsavari, R. Vajtai, P.M. Ajayan, Hexagonal boron nitride and graphite oxide reinforced multifunctional porous cement composites, Adv. Funct. Mater. 23 (2013) 5624–5630.
[222] T. Tong, Z. Fan, Q. Liu, S. Wang, S. Tan, Q. Yu, Investigation of the effects of graphene and graphene oxide nanoplatelets on the micro- and macro-properties of cementitious materials, Constr. Build. Mater. 106 (2016) 102–114.
[223] N. Sakhavand, P. Muthuramalingam, R. Shahsavari, Toughness governs the rupture of the interfacial H-bond assemblies at a critical length scale in hybrid materials, Langmuir 29 (2013) 8154–8163.
[224] M. Eftekhari, S. Mohammadi, Molecular dynamics simulation of the nonlinear behavior of the CNT-reinforced calcium silicate hydrate (C–S–H) composite, Compos. A: Appl. Sci. Manuf. 82 (2016) 78–87.